AMERICAN UNIVERSITY OF BEIRUT

STUDY OF SOME SPECIFIC FEATURES OF LIESEGANG PERIODIC PRECIPITATION, WITH APPLICATIONS TO GEOCHEMICAL PATTERN FORMATION

by
DALIA MOUSTAFA EZZEDDINE

A thesis
submitted in partial fulfillment of the requirements
for the degree of Master of Science
to the Department of Chemistry
of the Faculty of Art and Sciences
at the American University of Beirut

Beirut, Lebanon
September 2022

AMERICAN UNIVERSITY OF BEIRUT

STUDY OF SOME SPECIFIC FEATURES OF LIESEGANG PERIODIC PRECIPITATION, WITH APPLICATIONS TO GEOCHEMICAL PATTERN FORMATION

by

DALIA MOUSTAFA EZZEDDINE

Approved by:

Dr. Rabih Sultan, Professor
Chemistry
Advisor

Dr. Digambara Patra
Chemistry
Member of Committee

Dr. Mazen Al-Ghoul
Chemistry
Member of Committee

Date of thesis defense: September 2, 2022

AMERICAN UNIVERSITY OF BEIRUT

THESIS RELEASE FORM

Student Name:	Ezzeddine	Dalia	Moustafa
	Last	First	Middle

I authorize the American University of Beirut, to: (a) reproduce hard or electronic copies of my thesis; (b) include such copies in the archives and digital repositories of the University; and (c) make freely available such copies to third parties for research or educational purposes:

- ☐ As of the date of submission
- ☒ One year from the date of submission of my thesis.
- ☐ Two years from the date of submission of my thesis.
- ☐ Three years from the date of submission of my thesis.

Dalia Ezzeddine	September 15, 2022
Signature	Date

ACKNOWLEDGEMENTS

I would first like to deeply express my thanks to my supervisor Dr. Rabih Sultan for his constant support, patience, constructive feedback, and guidance through these projects.

I would also like to thank the research committee members, Dr. Digambara Patra and Dr. Mazen Ghoul for my thesis evaluation and their helpful feedback

I am grateful as well to Dr. Houssam El-Rassy for his valuable discussions.

Special thanks go to Miss Rania Shatila and Miss Manal Ammar for their help and support. Their help is highly appreciated.

I thank the Central Research Science Laboratory (CRSL) staff at AUB for continuous help with the instrumentations.

ABSTRACT
OF THE THESIS OF

Dalia Moustafa Ezzeddine for Master of Science
Major: Chemistry

Title: Study of Some Specific Features of Liesegang Periodic Precipitation, with Applications to Geochemical Pattern Formation.

Reaction-diffusion precipitation processes engender the formation of beautiful exotic strata of bands, in a way similar to the geochemical self-organization inherent in the morphology of some rocks. Liesegang patterning is one of the most well-known self-organization phenomena, governed by two pivotal processes which are ion diffusion and precipitation, taking place in a gel medium. An outer electrolyte reacts with an inner electrolyte in the gel during the interdiffusion of the two coprecipitates, exhibiting a beautiful display of rhythmic bands.

The present work is composed of three main sections: 1. A surface study of revert spacing in a 1D $PbCrO_4$ system; 2. Synthesis and characterization of calcium carbonate mineral during a carbonation reaction, carried out in a slaked lime gel matrix (mimicking a portlandite rock mineral); and 3. Chaos studies in a 2D Liesegang experiment with $PbCrO_4$ precipitation.

In the first section, we carry out surface and structural studies in a lead chromate Liesegang system exhibiting revert spacing in a 1D thin tube. Although the revert spacing phenomenon was fairly studied in the Literature, we demonstrated and confirmed in our study the ionic adsorption of chromate on the precipitate, and proved that the extent of adsorption increases with distance from the electrolytes junction. We used Scanning Electron Microscopy (SEM), Atomic Absorption Spectrometry (AAS), and Energy Dispersive X-ray (EDX) spectroscopic measurements. SEM micrographs revealed the presence of isolated particles at the bottom of a given band. These particles grow in size as we go down the tube, thus suggesting that adsorption increases. AA measurements confirmed the presence of free CrO_4^{2-} closer to the bottom of a band than the remainder of any interband gel portion. EDX measurements and calculations showed that the bottom of a band is always enriched with excess CrO_4^{2-}, and hence negatively charged, which causes the Coulombic attraction of Pb^{2+}, causing the next band to form closer and closer as we go down the pattern.

In the second section, we investigate the zonation of calcite [$CaCO_3$] in a portlandite mineral [$Ca(OH)_2$] putty, using a displacement reaction in the solid phase. The diffusion of aqueous carbonic acid into the portlandite-bearing putty causes the precipitation of calcium carbonate in a variety of patterns ranging from periodic (Liesegang) to mosaic (spherulites) patterns, attributed to the non-homogeneous distribution of calcium hydroxide particles after they first aggregate during the gelling. The differentiation of

the two minerals was characterized by pH measurements, Scanning Electron Microscopy (SEM), Fourier Transform Infrared Spectroscopy (FTIR), and notably powder X-ray diffraction (XRD), yet also distinguished to the naked eye by the phenolphthalein indicator color.

Finally, in the last section, we conduct experiments on $PbCrO_4$ precipitation in 2D Petri dishes, wherein the band distribution varies from periodic to deterministic chaos (yet to be rigorously characterized) within a flow rate range from 0.025 ml/day- 0.100 ml/day. Outside this range, periodic behavior was observed in the sense that 2D lead chromate pattern obeys the empirical scaling laws.

TABLE OF CONTENTS

ILLUSTRATIONS

Figure

TABLES

Table

CHAPTER I

INTRODUCTION

In nature, a wide range of self-organization examples exist abundantly in biological, physical, and geological systems such as concentric ring-like colony pattern in Proteus Mirabilis[1], rain water evaporation bands[2], stripe formation in rhyolitic stone[2], malachite marble[2], agate morphology[3], stripes on animal coats like zebras and mosaic colored patterns on butterflies' wings. Self-organization has many diverse applications in science. It is underlain by nonlinear dynamic scenarios and described by nonlinear dynamical equations, which are for instance fundamental in the dynamical formulation of the Liesegang phenomenon. Pattern formation occurs far from equilibrium in laboratory experiments or naturally. It is to be noted that self-organization does not violate the second law of thermodynamics which affirms that after any spontaneous change in the universe, the order of the universe will increase[4]. Thus, to compensate for the decrease in the order of the system due to self-organization, an increase in the entropy of the surroundings order will take place. In other words, the system orders itself at the expense of the surroundings.

Periodic precipitation is one of the most intriguing and interesting self-organization displays. It is well known as the Liesegang phenomenon[5-6]. Precipitate patterns were initially discovered by the German scientist Raphael Eduard Liesegang[7] in 1896. When an outer electrolyte solution of, say, silver nitrate ($AgNO_3$) is placed at the center of a gel medium containing an inner electrolyte of potassium dichromate ($K_2Cr_2O_7$) in a 2D Petri dish, the ions $Cr_2O_7^{2-}$ and Ag^+ interdiffuse in the gel medium, which leads to the formation of a silver chromate ($Ag_2Cr_2O_7$) rings pattern, manifested as

an alternation of precipitate zones and precipitate- free space. Plenty of examples of Liesegang banding[2, 6] are found in the literature.

A typical Liesegang experiment represents an open system where the precipitates get formed through a diffusion-precipitation process, wherein the diffusion of the reactants is driven by the concentration gradient; whereas the precipitation is caused by exceeding a nucleation threshold. Within the gel medium (Gelatin, Bacto Agar, Agarose, Starch, Silica), precipitate patterns were produced[8]. The gel matrix has a great importance such as to support the crystals formed without exerting forces upon it, to eliminate the occurrence of convection process, and to suppress nucleation. Many factors affect the dynamical properties and the morphological characteristics of the precipitate patterns, such as the gel concentration[9], inner and outer electrolyte concentrations[10], the presence of another competitor ion[11], temperature[9], and impurities[12-13].

A. Precipitate Patterning Systems and Theories

For over a century, reaction-diffusion precipitation processes have been studied, but the mechanisms which are the basis of the formation of Liesegang patterns are still under debate. Therefore, scientists did not succeed in arriving at a universal explanation of the experimental findings due to the lack of experimental evidence. The Liesegang patterning morphological properties are characterized by some empirical scaling laws (spacing law, width law, and time law), and have been modeled by some theories (essentially pre-nucleation and post-nucleation theories). We start by introducing the time law, the width law, and the spacing law, then we present the pre-nucleation and post-nucleation theories.

In the 19th century, due to the diffusion motion of an outer electrolyte in a gel medium containing an inner electrolyte, the time law is generated [14-15] which is an empirical law that correlates a certain band formation time (t_n) to its position (X_n)

$$X_n \sim (t_n)^{1/2} \qquad \text{(Equation 1.1)}$$

A plot of x_n versus $t^{1/2}$ typically yields a square root diffusion curve[16].

As the number of bands (n) increases, the x_n^2/t_n ratio usually approaches a constant value. Morse and Pierce[15] discovered this law which illustrates the progression of the Liesegang patterns produced with time as shown in equation 1.2, where β_0 and γ_0 are constant values.

$$X_n = \beta_0 (t_n)^{1/2} + \gamma_0 \qquad \text{(Equation 1.2)}$$

Liesegang banding systems present special features, and are divided into two main categories from the viewpoint of morphological appearance: direct[6, 17] and revert spacing[5] systems, with the former being based on Jablczynski's spacing law[17]. Direct spacing denotes Liesegang systems wherein the distance between two consecutive bands increases as we move away from the electrolytes junction (both in 1D and 2D); whereas in revert spacing systems, the spacing between two consecutive bands decreases with distance from the interface. Examples of direct and revert spacing Liesegang systems are illustrated in Figure 1.

This spacing law[17] is only applicable for direct spacing Liesegang systems. It applies for only large n values and it expresses that the ratio of the position of two consecutive Liesegang bands should be nearly equal to a constant value denoted by "1 + p", where p

is known as the spacing coefficient. This latter depends on the inner and outer electrolyte's concentrations[18], and is usually between 0.05 and 0.4.

$$\frac{x_{n+1}}{x_n} = 1 + p \qquad \text{(Equation 1.3)}$$

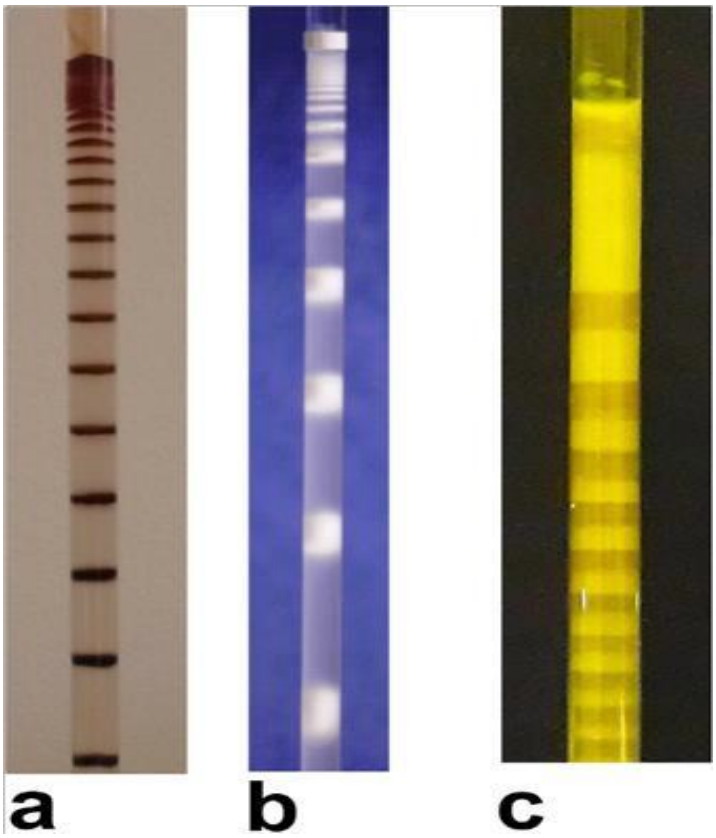

Figure 1. Three distinct Liesegang patterns: (a) Silver dichromate system (Ag_2CrO_7); (b) Magnesium hydroxide system ($Mg(OH)_2$); (c) Lead chromate Liesegang system ($PbCrO_4$). The last one (c) follows the revert spacing trend, however, the first two systems exhibit direct spacing.[19]

The above spacing law was adjusted by Mathur[19-20] as expressed below:

$$x_{n+1} - x_n = a\left(\frac{S}{C_0 C_0^{F}}\right) \exp(\alpha x_n) \qquad \text{(Equation 1.4)}$$

Where a and α are constants, S represents the solubility product, C_0 and C_0' represent the outer and inner electrolytes' initial concentrations respectively, and

x_{n-1} and x_n are the positions of the $(n-1)^{th}$ and n^{th} Liesegang bands from the electrolytes junction. For a direct spacing system, α is positive, while it is negative for a revert spacing Liesegang system.

The width law[21] is another empirical law that applies to Liesegang systems. This latter relates the width of the Liesegang patterns with the number of patterns n. It states that with increasing the number of bands n, the width of the patterns W_n increases as well. This is only applicable in direct spacing Liesegang systems, interestingly, whereas the opposite is true in revert spacing Liesegang systems.

$$W_n = \varepsilon X_n \qquad \text{(Equation 1.5)}$$

1. Pre-Nucleation Theories

a. Supersaturation Theories

In 1896, Wilhelm Ostwald[22-23] suggested a theory nowadays referred to as the "Ostwald's supersaturation theory" to explain the formation of Liesegang patterns. This theory is considered the bulk and essence of the pre-nucleation theories[22, 24-26]. It represents the simplest and the most important model of Liesegang banding. It does not involve the formation of any intermediate steps. After half a century, Prager[27] proposed a mathematical formulation for the model proposed by Ostwald and then it was later reformulated by Wagner[12]. Ostwald's theory is built on a series of events in the site where the concentration profiles of the two coprecipitate ions meet:

1. Supersaturation in the interdiffusing co-precipitate ions of the inner and outer electrolyte in some zone of the electrolytes junction
2. Nucleation of particles that lead to the formation of precipitate a band
3. Depletion of the diffusing reactants for a certain interval of time

These steps are repeated to form a continuous cycle named the Ostwald cycle (or supersaturation- nucleation- depletion cycle).

The mechanism behind the formation of Liesegang bands is the diffusion of an outer electrolyte O into a gel medium containing the counter-ion precipitate I (inner electrolyte) coupled with a precipitation reaction that leads to the formation of precipitate P without the intervention of any intermediate.

Outer Electrolyte (O) + Inner Electrolyte (I) $\longrightarrow$ P (precipitate pattern)

Initially, the two co-precipitate ions should be present in a supersaturated zone before a precipitation reaction occurs. When the reactant concentrations product [O][I] exceeds a threshold value I* (called the supersaturation), nucleation of the precipitate pattern (P) occurs at this site. An equation representative of the supersaturation assumption proposed by Ostwald at position x and time t is shown below:

$$O\,(x, t)\,I\,(x, t) \geq I^* \qquad \text{(Equation 1.6)}$$

where I* is the supersaturation, as defined above.

As the particles grow in size, the first band gets formed. Thus, the nucleation process is suppressed, and the concentration of the reactants gets depleted very fast. With time, the ions of the outer electrolyte solution continue to diffuse within the gel medium containing the counter-ion precipitate until the threshold value l* is reached again. As a result, the nucleation particles get bigger, which engenders the formation of a second precipitate pattern. As time proceeds and as the supersaturation-nucleation-depletion cycle is repeated, the concentration of the outer electrolyte becomes more dilute that

triggers the formation of patterns further away from the interface. Thus, the spacing between two consecutive bands gradually increases as we move away from the electrolytes junction. It is true that the "Ostwald Prager Theory" is considered the most accepted and valid theory to explain Liesegang patterning phenomena, however, it presents some drawbacks based on macroscopic observations as below:

1. It is not applicable for revert spacing systems wherein the spacing between two consecutive bands decreases as we move away from the interface. Such behavior is observed in $PbCrO_4$[19, 28-30], HgS[31-32], AgI[29, 33], Ag_2CrO_4[34-35], CuS[36-37] Liesegang systems.
2. It cannot explain the formation of secondary structure bands. I observed such behavior in $Ag_2Cr_2O_7$ Liesegang system in 1D test tube.
3. It prognosticates Liesegang bands should have an unbelievably zero-width.
4. It cannot provide an explanation for post-nucleation patterning observed in many Liesegang experiments. Some experiments showed that to form a band, nucleation is not a primary condition. Magnesium hydroxide ($Mg(OH)_2$) periodic patterns in gelatin gel medium for instance were observed due to the breakup of a colloid's continuous region, a long interval of time after nucleation process has occurred[38-39].

5. Phase Separation Theories

As mentioned earlier, the supersaturation model was incapable to explain many macroscopic features of periodic patterns obtained from a Liesegang experiment, a new theory was suggested. Phase separation engenders an alternation of high- and low-density

zones that is the basis of the formation of an intermediate followed by the formation of periodic Liesegang bands[39]. According to this theoretical approach, the formation of an intermediate is an essential step preceding the formation of a precipitate pattern[39]. An equation representative of the diffusion front's position is shown as below:

$$X_f = (2D_f t)^{1/2} \qquad \text{(Equation 1.7)}$$

Where X_f is the position of the diffusion front, D_f represents the diffusion coefficient (cm^2/s), and t represents the time (s).

6. Adsorption theory

Bradford[40] proposed another pre-nucleation theory to explain the Liesegang banding phenomenon. His theory is based on the adsorption process of the inner electrolyte by the precipitate particles, which leads to the formation of free space regions between the concentric rings (2D). According to Bradford[40], the adsorbing capacity of the precipitate is determined by the percentage of its dispersion. Adsorption is high when the particles are small and a pattern will form. However, when the particles are large, adsorption is small and the pattern formation will not occur. He also demonstrates the effect of the gel on the crystals' growth and underlines the importance of adsorption of the diffusing reagents onto the internal surface walls of the cell[41].

Bolam et al.[42] suggested another pre-nucleation model to explain the formation of Liesegang patterns. He demonstrated that the spacing between bands were formed due to Coulomb repulsion between the free ions and the diffusing ions adsorbed on the precipitate. According to his model, the distance between the last band and the ions

diffusing from the outer electrolyte should be large enough for precipitation to occur and hence repulsion forces to be negligible[42].

7. Sol Coagulations theories

The supersaturation and the sol coagulation models are almost the same, except that in this theoretical approach, there is the formation of colloidal species C. Therefore, another theoretical model is introduced to explain the formation of the obtained bands.

This theory is based on two essential steps:

1. The formation of a microscopic colloid
2. The appearance of a precipitate pattern

2. Post- Nucleation Theories

Due to the limitations of the pre-nucleation models in providing a complete justification for the appearance of different types of obtained precipitate patterns, two post-nucleation theories[43-44] were introduced in the literature: competitive particle growth (CPG) theory[45] and flocculation theory. The first model[44] is based on Ostwald Ripening scenario[46].

In 1978, Feinn et.al[45] postulated the competitive particle growth model (CPG) that is also well known as the aging or coarsening theory. They performed experiments on lead iodide (PbI_2) Liesegang systems to show that the coupling of the diffusion process to the autocatalytic growth of colloidal species leads to a chemical instability in the tug between particle sizes: the small crystals (having high solubility) are dissolved to the advantage of the production of few large particles (having low solubility), because the larger crystals possess a large surface-to-volume ratio[38]. When the system continuously

evolves toward the development of a smaller amount but bigger crystals, this process is called the Oswald Ripening Process[46]. As the large particles continue to grow and evolve further, they become surrounded by a depleted region of small colloidal crystals, which engenders an alternation of parallel precipitate patterns and precipitate free regions[38]. The The group of Ortoleva[43] successfully solved the reaction-diffusion equations, by incorporating the effect of the dissolution equilibrium constant on particle size, and hence reproduced the alternation between precipitate and precipitate-free zones. Post-nucleation scenarios have been reported in the literature and applied to distinct Liesegang systems such as magnesium hydroxide ($Mg(OH)_2$)[38, 47] and lead iodide (PbI_2)[38, 45] systems. This theory is based on the principle that nucleation takes place before the formation of banded precipitate structures (i.e. not simultaneously). At first, as the outer electrolyte diffuses within the gel containing the inner electrolyte, nucleation of a homogeneous colloidal set of crystals is followed by the continuous competitive particle growth that leads to the development of periodic precipitate patterns. In the second theory, coagulation is a process that occurs when the total concentration of the ionic product is above the flocculation threshold value. However, it is unable to justify the formation of few space-free areas between every two consecutive precipitate bands (or rings) in Liesegang systems.

Flicker and Ross[39] postulated the below model even if the concentration gradient is not present. A general scheme representing how the bands get formed using this model is shown below:

$$O + I \longrightarrow C \qquad \text{(Equation 1.8)}$$

$$C \longrightarrow P \qquad \text{(Equation 1.9)}$$

$$C + P \longrightarrow 2P \qquad \text{(Equation 1.10)}$$

Where O, I, C, and P are the outer electrolyte, inner electrolyte, colloidal species, and precipitate, respectively. Initially, an outer electrolyte diffuses into a gel medium containing a counter ion precipitate until a nucleation threshold value is reached (l*).

Due to the continuous diffusion of the outer electrolyte into the gel medium, the concentration of the outer solution starts to accumulate in the matrix which will increase the concentration of the ion product until a critical threshold is reached (C*). As a result, the concentration of the sol is also above this critical value (C > C*). The presence of the precipitate (P) triggers the reaction between the intermediate sol (C) and the precipitate to produce 2 P, as shown in equation 1.10. This last step is known as the autocatalysis process that engenders the formation of precipitate patterns. The incorporation of the sol particles into the obtained precipitate pattern engenders the occurrence of a depleted zone of sol particles. The consumption of all available colloidal species (colloidal intermediate) will stop the production of P. There, the last step will turn the process off and no bands are observed anymore. As time proceeds, the ions of the outer electrolyte solution continue to diffuse within the matrix until the critical threshold is reached again which leads to the appearance of consecutive bands. Although this model explains qualitatively the pattern formation, it was proved to suffer from major computational limitations.

Dhar and coworkers[5] demonstrated that the coagulation of a peptized solution leads to the formation of Liesegang patterns. They showed that some reactants can be peptized in the presence of a gel matrix and beautiful patterns can also be observed such as silver bromide, silver chloride.

Hedges and Henley[48] supported this model by managing to isolate the chemical reaction region from the precipitate patterns formed within a certain concentration range. According to the sol coagulation theory, the precipitate bands formed are due to the formation of a colloidal sol followed by the chemical reaction front. Ross and Müller[48] also confirmed the production of a colloidal sol preceding the formation of a precipitate band by performing several other experiments.

This theory is only applicable to a classical Liesegang system. Liesegang experiments that lead to the formation of dynamic precipitate bands cannot be explained using this model. This proposed model cannot explain revert spacing and secondary structures Liesegang bands.

3. Applications

Several fascinating applications of Liesegang phenomena that exist in nature have been reported in several studies in biology[2, 49], bacteriology[2, 50], and specifically geology[2, 4, 51]. The primary resemblances between concentric rings formation in non-living systems and bands formation in living systems are observed in the performance of bacteria and the development of their colonies. Bacillus (B.) subtilis[52-53] is one of the examples of bacteria that forms concentric rings colonies. Ohgiwara, Matsushita, and Matsuyama performed the morphological phase diagram to demonstrate five distinct colony patterns for this bacterium[53]. At first, bacteria extend in a circular way searching for food in the gel matrix. Then, bacteria consume nutrients available in the medium to grow and aggregate at a later stage. The formation of a concentric ring is due to the high level of nutrients found in the matrix, although the level of agar is reduced. Concentric rings patterns formation is built on two phases:

1. Migration phase

2. Consolidation phase

In the first phase, the bacteria are actively moving searching for nutrients that leads to the growth and expansion of the bacterial colonies. In the second phase, the colonies stop growing noticeably. Each phase lasts for around 2-3 hours. These 2 phases are repeated in a continuous cycle that leads to the formation of concentric ring-like colonies.

Knöll and Schmidt[6] also reported close analogies between Liesegang rings obtained by the classical Liesegang experiment performed in the gel and the expansion of bacterial colonies. Figure 2 clearly shows a similarity between the concentric rings patterns (left) produced by P. mirabilis[54], and those obtained in a lead chromate precipitate pattern (right) obtained from a classical Liesegang experiment in gel medium.

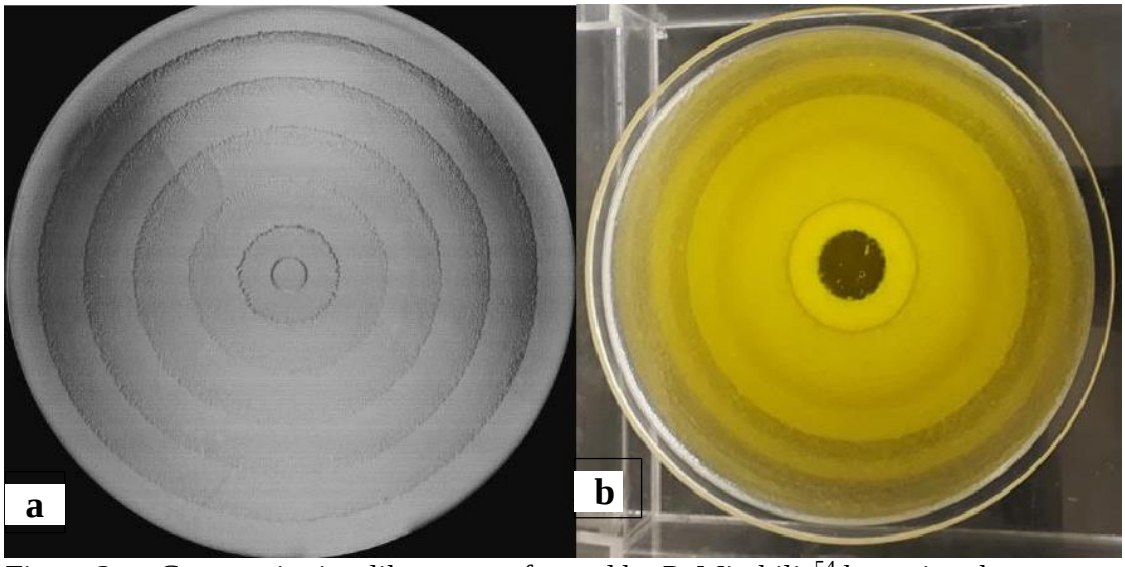

Figure 2. a. Concentric ring-like pattern formed by P. Mirabilis[54] bacterium.b. Precipitate patterns formed by a lead chromate ($PbCrO_4$) Liesegang system. Note the analogue between the two systems.

In the last three decades, geologists have increased their focus of studies on the theories of Liesegang banding to explain the formation of stripes in a wide variety of rocks as well as in agates and geodes. Liesegang himself reported the appearance of strata of patterns in a wide variety of rocks that characterize their textures. Figure 3 shows similarities between a cobalt hydroxide $Co(OH)_2$ pattern and the banding structures in the form of rings in real, natural rock systems: a Liesegang stone (frame a), also called the rhyolitic stone, and malachite marble (frame c)[2].

This thesis is composed of three main parts (separate studies): a surface study of revert spacing, the carbonation reaction of a slaked lime gel matrix, and chaos studies in 2D Liesegang experiments.

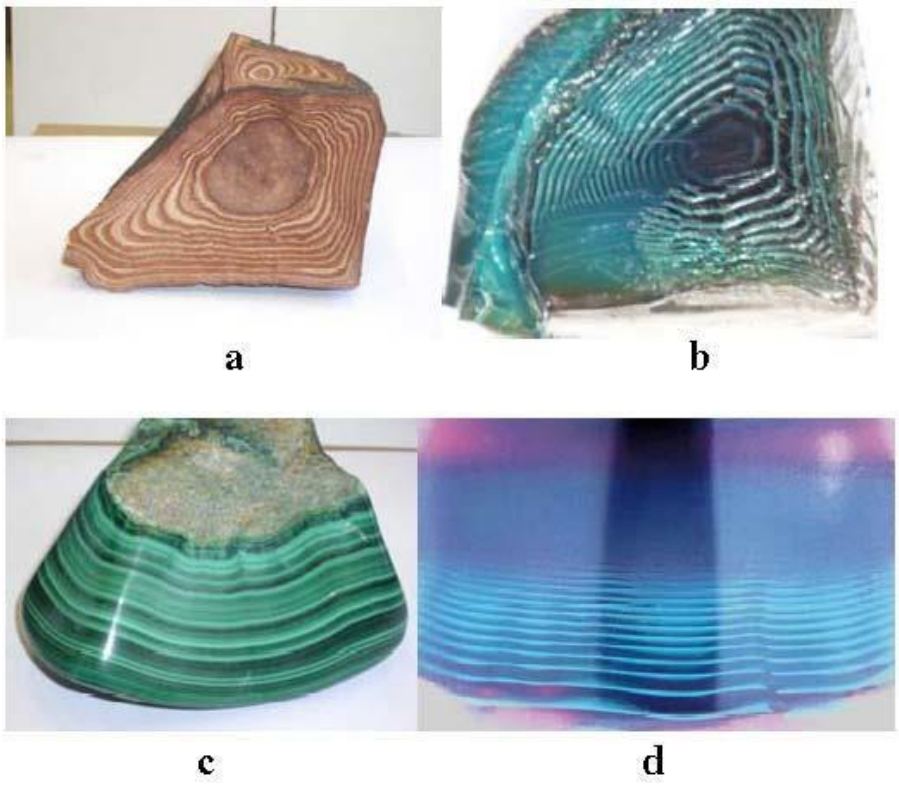

Figure 3.a. Striped Rhyolite stone; b. $Co(OH)_2$ concentric rings patterns observed in a 3D gel medium, similar to the bands observed in the frame a; c. Strata of patterns in

malachite marble; d. $Co(OH)_2$ patterns expand at the bottom of an Erlenmeyer, resembling the patterns in stone c[2].

B. Special features: Review of Revert Spacing in the Literature

Several Liesegang systems exhibiting revert spacing were notably reported in the literature such as AgI[29], AgBr[55-56], CuS[37], CdS[57], $PbCrO_4$[19, 28], HgS[32], $Fe_3[Fe(CN)_6]_2$[58]. Revert spacing systems are less frequent in the literature, but they are gradually becoming more frequent.

Revert spacing is explained by some mechanisms that there are still under debate, to explain the formation of rhythmic bands becoming closer to each other as opposed to systems where they develop farther and farther apart.

In 1925, Hatschek[59-60] studied the effect of light on lead chromate Liesegang systems. He demonstrated that the spacings between two consecutive bands were different when lead chromate Liesegang systems were exposed to light and in darkness[59]. In 1958, Ghosh and Mathur[61] proposed that the capability of the outer electrolyte to diffuse, dissolve out or peptize the precipitate promoted the revert spacing mechanism. In 1974, Flicker and Ross[58] postulated that with increasing distance from the gel boundary, the concentration of the colloid sol and the diffusion coefficient decrease, and hence revert spacing system was supported. Their postulation is based on instability from a homogeneous and colloidal suspension due to autocatalytic particle growth.

In 1981, Ramasamy et. al[29] performed a silver iodide Liesegang experiment (AgI system) to explain revert spacing on one hand, and the transition from revert to normal

spacing on the other, using a theory based on the colloids stability and DLVO[1] theory. This theory is based on the charge on the sol particles. In 1984, the same group studied two other Liesegang systems, which are lead chromate ($PbCrO_4$) and Cadmium Sulfide (CdS) to test a proposed theory based on the preferential adsorption of the diffusing co-precipitate ion[57]. In 1988, Das et.al [62-63] postulated a mechanism to prove that light induces lead chromate periodic precipitation, and affects the growth of lead chromate crystals. In 1994, Müller et. al[64-65] proposed a more advanced mechanism based on the particle growth from colloid, and on the post-nucleation scenario.

In 2011, Karam et. al[28] investigated a $PbCrO_4$ Liesegang banding system exhibiting revert spacing as shown in Figure (Fig. 1c)[19]. They studied the morphological properties of the lead chromate revert bands and contrasted that system with a direct spacing copper chromate ($CuCrO_4$) Liesegang system. They employed UV spectrophotometry to demonstrate the increase in the adsorbed CrO_4^{2-} ions on the successive lead chromate bands. In the present work, we will continue this latter study via novel surface and structural investigations in a lead chromate patterning system exhibiting revert spacing, presented in Chapter II. We aim at supporting and providing evidence for the role of adsorption mechanism in the formation of lead chromate revert patterns, by utilizing different techniques such as EDX, SEM and AAS[19].

C. Analogy with Geochemical Self- Organization

Geochemical self-organization is well studied, and has notably grown especially in the second half of the past century[66-69]. This terminology mostly refers to the similarity relation between Liesegang banding and geological patterning. In

1 Derjaguin, Landau, Verwey and Overbeek

geological systems, beautiful rhythmic bands formation is observed and encountered in a variety of rocks[67]. The lithosphere's morphology is illustrated by several distinct characteristic patterns classified from Liesegang rhythmic bands[6, 70-72] to geodes, agates[73-74], orbicules[75-76] and concretions[77-78]. The literature is rich in examples of other mineral patterns linked to the Liesegang phenomenon such as octocalcium phosphate patterns, zebra stone, iron oxide mineral bands, etc. Different mechanisms focusing on the rock's physico-chemical characteristics were proposed to explain various phenomena such as metamorphic layering and oscillatory zoning[4]. The periodic patterning phenomenon can occur within geological medium due to the precipitation processes as was highlighted by Liesegang himself.

In previous works, sedimentation of infused matter was the basis to explain periodic banding in rocks. But, another possible explanation should be taken into consideration since it is observed that spherical concentric rings could be superposed on a homogeneous background. Nowadays, computational techniques are employed to model geochemical self-organization and to simulate solutions[4].

In material science and engineering, specifically in concrete research, carbonation of lime cements is of pivotal importance[79-80]. Two important processes play an important role in the destruction of mortars, monuments and the deterioration of building of stones: cementation and carbonation[81]. This latter is well known as the differential erosion[81]. An assessment of the kinetic and thermodynamic characteristics of the below carbonation equation (1.11) within the medium should be performed to determine the capability of a portlandite concrete to resist erosion. Thus, to maximize this resistance, a concrete mixture should be reinforced with a dense, low porosity and

impermeable microstructures that can be guided by the control of such physicochemical parameters.

$$Ca(OH)_2\,(s) + CO_2\,(aq) \longrightarrow CaCO_3\,(s) + H_2O\,(l). \qquad \text{(Equation 1.11)}$$

In a previous work, Msharrafieh et al.[82-83] carried out a novel study on the diffusion process of an acidization front (H_2SO_4) invading inside a limestone ($CaCO_3$) rock medium.[83] Calcium sulfate (anhydrite or gypsum) layered deposition was obtained and further studied. As the diffusion front evolves from a central source of sulfuric acid, oscillations in the amount of deposited calcium sulfate was observed, delineating a clear and distinct zonation, with a typical morphological appearance of an aged rock.

In 2002, Rodriguez-Navarro et al.[69] performed a study on a portlandite [$Ca(OH)_2$] putty treated with water containing intermediate levels of carbon dioxide (carbonated water). Liesegang banding in the calcium carbonate content (calcite) was obtained just like within a real portlandite rock medium. The conversion of calcium hydroxide [$Ca(OH)_2$] to calcium carbonate [$Ca(CO_3)$] is due to a displacement reaction in the solid phase according to the above chemical equation (1.11). This is what makes this study particularly interesting, and triggered our further investigation.

Guided by the work of Rodriguez-Navarro et al., we performed a study on the formation of calcium carbonate patterns by immersing a slaked lime of calcium hydroxide [$Ca(OH)_2$] gel putty into an outer solution of carbonic acid (H_2CO_3) by forging the displacement reaction (1.11), in addition to its exposure to atmospheric CO_2. The performed process gave rise to a variety of patterns, ranging from Liesegang bands to mosaic patterns.

D. Chaos

In a wide variety of natural and non-natural dynamical dissipative systems, chaotic patterns could be observed. This latter behavior can be found in the heart and brain of living organisms, in solar systems, and meteorology[84]. It is also known as aperiodic behavior. Non-linear natural dynamical systems and stochastic driving forces are two different main sources that leads to nonperiodicity. Any possible source of noise in the experimental initial conditions or random fluctuations could engender nonperiodicity denoted as stochastic behavior[65, 84], and therefore cannot be considered as deterministic chaos. In 1972, Edward Lorenz, a meteorologist, who integrated the phenomenon of Chaos theory into the modern world by giving an interesting example of aperiodic behavior in nature.[85] He proposed a mathematical model to describe how air moves in the atmosphere[84]. Such early work influenced another pioneer on Chaos theory, Otto E. Rössler, who introduced a simple chaotic model in 1976[86]. He later published a study on Chaos in the Belousov-Zhabotisnkii reaction in 1978[87].

In 1989, Chaos theory proposed by Devaney[88] suggested that a small change *now* will result in a massive change *later*. His theory affirmed that a slight modification in the initial conditions can yield to vast and diverse outcomes for chaotic systems[84].

The repetition of an array of similar units with a specific or unspecific symmetry is defined as pattern formation. This repetition can be periodic or aperiodic. Periodic and aperiodic behaviors are notably observed in a variety of natural and chemical systems. It is thus the role of the chemist to analyze, by standard techniques, whether an observed aperiodicity is stochastic (random fluctuations) or deterministic chaotic.

In chemical systems, the prediction of gas solubility is an important criterion to manufacture polymers, but models using particle swarm optimization (PSO) tend to

converge to the wrong points. By introducing chaos, an updated version of PSO has been invented which keeps the simulations from being unable to move further[84]. Another typical illustrative example is the Belousov-Zhabotinskii (BZ) reaction[89]. The latter shows a complex intriguing behavior when kept unstirred in a cuvette environment. As the system progresses in time, there is a transition from periodic to chaotic, and a return back to periodic[89]. Due to reaction decoupling, diffusion, and convection, this transition in the BZ reaction is observed. Another chemical reaction in which the pH varies chaotically with time is the hydrogen peroxide sulfur IV hydrogen carbonate flow system[90] . Paradigms on chaos in physico-chemical systems are ubiquitous. One example which illustrates chaotic behavior is in the study of a high order numerical scheme for fractal-fractional laser system[91], wherein the dynamical behavior of a fractional and fractal-fractional (FF) order laser chaotic model is investigated. This model is initially considered with an iterative technique based on Laplace transform.

Rössler et al.[87] established chaos in the BZ reaction by monitoring three variables, first triggered by the observation of a complicated limit cycle. He noted that such a state space multiply folded limit cycle is in itself, an indicator or a precursor for the existence of chaos. In general, the evidence for chaos in the BZ reaction lies in the manifestation of 'double oscillations' in continuous stirred flow conditions.

In physiological systems, many dynamical systems which exist in the human body exhibit rhythmical movement such as the beating of the heart, the circadian rhythm of walking and sleeping, the regular cycle of inhaling and exhaling air that makes up breathing[84]. These dynamic systems are not always perfect and sometimes undergo a period of chaotic behavior. In order to reduce sleep disorders, heart disease and mental disease, chaos theory is applied to human dynamical systems[84]. Cardiac arrhythmias are

instance of chaos. In 1992, Garfinkel, Spano, Ditto and Weiss developed a method called proportional perturbation feedback (PPF) to control arrhythmia[92]. This method was effective to restore a periodic rhythm and provide a less dramatic invasion into the patient's system[92].

In celestial mechanical systems, when planetary scientists observe especially asteroids and they apply chaos theory, this will lead to better estimations about when these objects will approach other planets and Earth. Pluto's four or five moons rotate chaotically[89].

In previous work, Mustafa Saad et al.[93] carried out an interesting study on the diffusion process of ammonium hydroxide (NH_4OH) invading inside a doped gel containing Cobalt ions (Co^{2+}). Thus, cobalt hydroxide patterns ($Co(OH)_2$) were obtained and further studied. The diffusion of NH_4OH solution coupled to precipitation and redissolution, induced oscillations in the number of bands were obtained due to the redissolution of the bands in high NH_4OH concentration, which was proved to exhibit characteristic, deterministic chaotic behavior, as shown in figure 4.a. In this system, chaotic behavior is observed through diffusion-precipitation-redissolution reactions[93].

In our present study, we performed a study that targets lead chromate ($PbCrO_4$) patterns in 2D that do not obey neither the spacing nor the width laws (in the sense that they become aperiodic) by delivering continuously an outer electrolyte of potassium chromate (K_2CrO_4) at a very slow flow rate, after an initially constant diffusion source that nourishes the gel.[94] The performed process gives rise to patterns that vary in number, thickness, and spacing under specifically controlled flow rate,[94] and display aperiodic behavior.

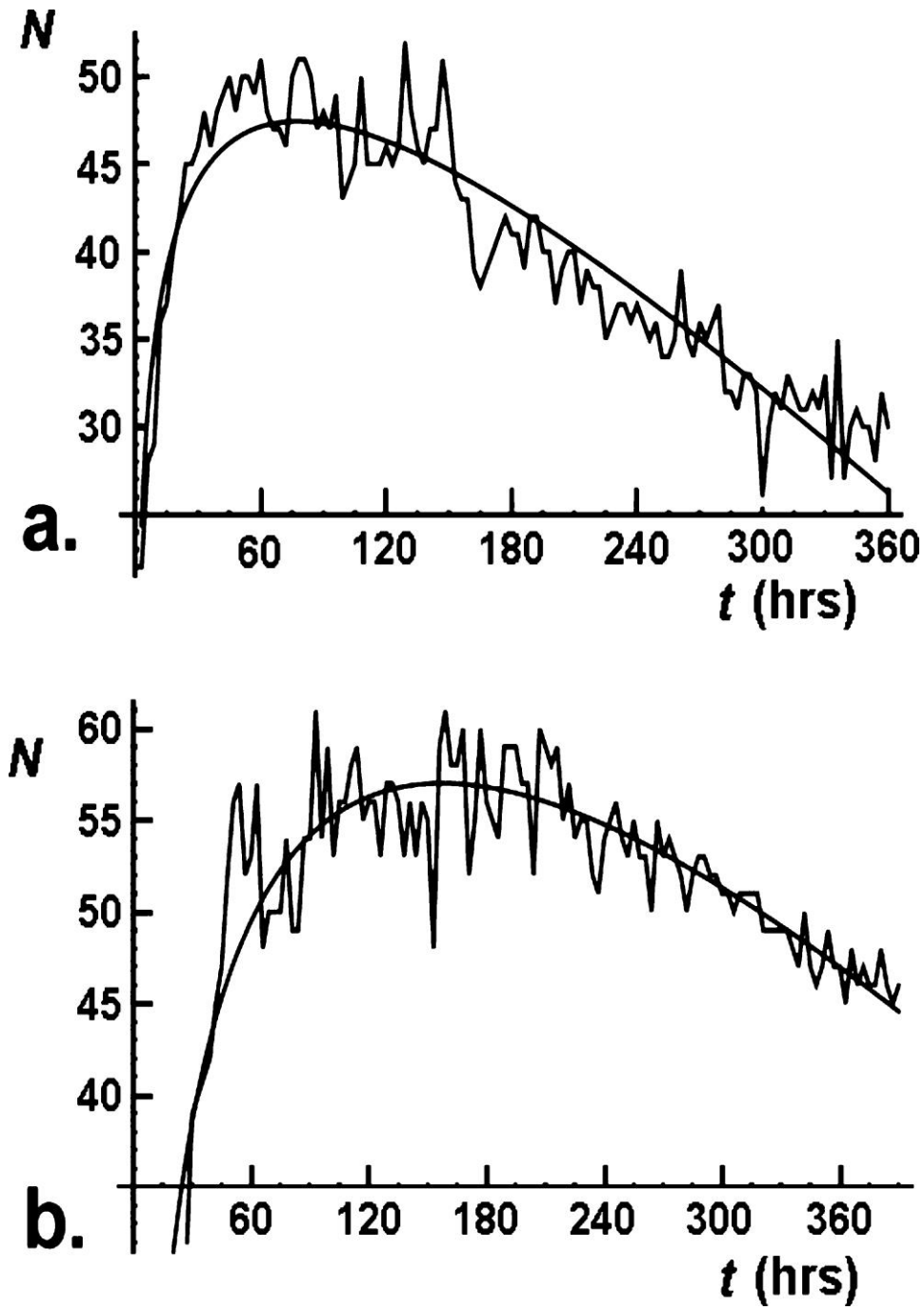

Figure 4a. Chaotic behavior of the number of the bands (N) vs time (hrs) for two different inner concentrations (a) $[Co^{2+}]_0$ = 0.30 M; (b) $[Co^{2+}]_0$ = 0.10 M; outer electrolyte $[NH_4OH]_0$ = 13.3 M. Both plots exhibit first an increase, reach a maximum, then an overall decrease.[93]

E. Aims of the Study

The main aims of the present study are summarized as follows:

1. Carry out a novel, surface and structural study of revert spacing in 1D $PbCrO_4$ Liesegang pattern using SEM, EDX, and AAS techniques to investigate the effect of adsorption of CrO_4^{2-} on the precipitate in explaining revert spacing.
2. Study the formation of calcium carbonate precipitate patterns during the carbonation reaction of a slaked lime gel matrix, using several techniques (SEM, IR, XRD).
3. Study Chaos in 2D Liesegang experiments with $PbCrO_4$ precipitation, wherein the band distribution experiences a transition from periodic to deterministic chaos.

CHAPTER II

A SURFACE AND STRUCTURAL STUDY OF REVERT SPACING IN A 1D $PBCRO_4$ LIESEGANG SYSTEMS

As mentioned earlier, many theoretical models exist in the literature trying to explain the revert spacing mechanism in Liesegang experiments. There is no complete, unified theory to justify the formation of revert patterns due to the scarce experimental evidence. Thus, there is no final and decisive model for the obtained patterns exhibiting revert spacing.

A previous study was performed by Karam et al.[28] to study the morphological characteristics of revert lead chromate precipitate patterns using UV spectrophotometry. We aim to pursue this study to provide evidence for the role of adsorption by performing novel surface and structural investigations in the $PbCrO_4$ system using techniques such as EDX, SEM, and AAS[19].

A. Experimental Method

1. Lead chromate ($PbCrO_4$) pattern synthesis

A sample of $Pb(NO_3)_2$ of concentration 0.00100 M (Fluka, 99.0%; weighed to the nearest 0.0165g), was dissolved in 50.00 mL of double distilled water with the desired amount of Bacto agar powder (1% w/w Bacto agar gel). The mixture was heated to 85˚C under constant stirring until a homogeneous solution was obtained. The resulting solution was then poured into a set of 1D glass tubes, filling each to two-thirds. The solution was left to solidify for six hours at room temperature. Afterwards, an outer electrolyte of concentration 0.20 M (K_2CrO_4; Fluka, 99.0%) was gently poured on top of the lead

nitrate-doped gel. The tubes were then covered with parafilm and exposed to sunlight at room temperature.

2. Preparation for Analysis

After the lead chromate patterns were formed, we cut the test tube at the bottom to take out the gel meticulously. The latter was extracted in a perfect sliding process. We then performed a careful separation of the bands, as well as the interband regions to study their morphological characteristics and their and chemical composition. The samples obtained were characterized using EDX, SEM after coating the samples with a thin layer of gold (15 nm thickness); and AAS, conducted on a SOLAAR atomic absorption spectrophotometer.

B. Results

1. Scanning Electron Microscopy (SEM) Studies

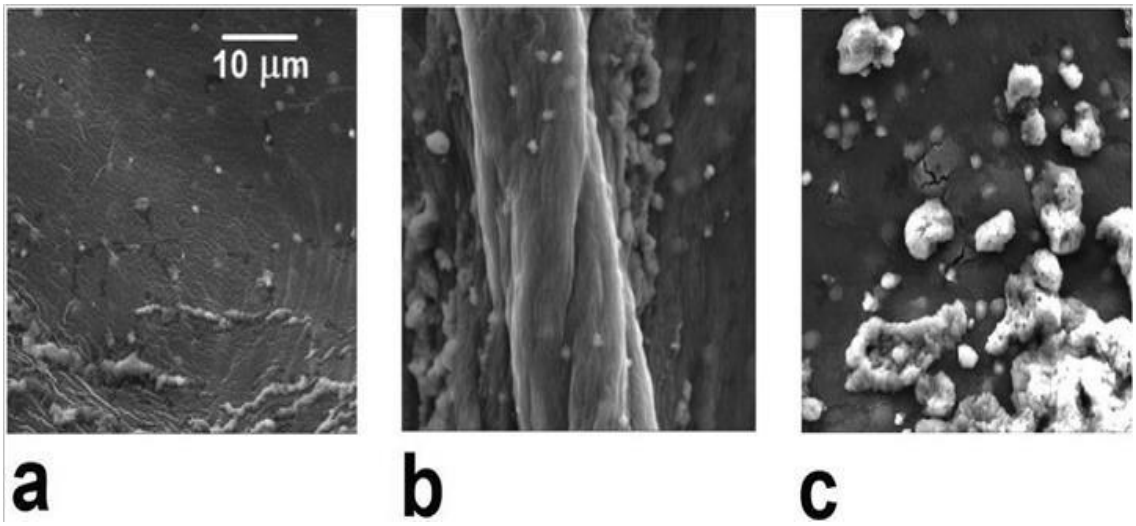

Figure 5. Scanning electron micrographs for three consecutive bands in a lead chromate ($PbCrO_4$) Liesegang pattern exhibiting revert spacing. (a) band 1; (b) band 2; (c) band 3.[19]

A typical appearance of the lead chromate system, exhibiting revert spacing is shown in Fig.1c. As we move away from the electrolyte junction, a decrease in the spacing between the lead chromate bands is observed. The spacings for three selected interband portions were measured as 0.80, 0.70 and 0.55 cm respectively as we move further from the interface, depicted in Fig. 6a.

In previous work, the lead chromate patterns characteristics and phenomenology were analyzed[28, 95]. By spectrophotometric measurements, it was shown that the fraction of adsorbed chromate ions (CrO_4^{2-}) increases as the band number increases. We here study the surface and morphological characteristics of the bands. SEM micrographs of the bottom of the first three bands, labeled a, b and c respectively, are shown in Fig. 5.[19] As we go from band 1 to band 2 to band 3, we can clearly recognize different isolated particles embedded within the texture, whose size notably increases.[19]

Those particles correspond to isolated $PbCrO_4$ deposits onto chromate ions (CrO_4^{2-}) aggregates, adsorbed on the lead chromate precipitate. The size of the different isolated particles increases as we move away from the junctional surface and this finding is in congruence with the Ostwald ripening phenomenon. According to the equilibrium shown below, in the interband region, the lead ions were demonstrated to be divided between free Pb^{2+} and the complex Pb^{2+}- $PbCrO_4$ complex.[19] This latter complex was identified by mass spectrometry[95].

$$Pb^{2+}(aq) + PbCrO_4\,(aq) \rightleftharpoons Pb^{2+} - PbCrO_4\,(aq) \qquad \text{(Equation 2.1)}$$

The free Pb^{2+} are positively charged ions and they are attracted to the negatively charged ions which are the adsorbed CrO_4^{2-} by columbic forces. Then, $PbCrO_4$ precipitate is deposited as the isolated particles appearing in Fig. 5.[19] When more CrO_4^{2-} diffuse into the gel doped by Pb^{2+} ions, these ions will be displaced from the complex $Pb^{2+} - PbCrO_4$ (aq). Therefore, a second band will be formed closer to the first band due to the columbic attractions mentioned before. One further evidence also supporting this mechanism, is that after removal of the gel from the aqueous interband region to be analyzed by AAS, the free Pb^{2+} were completely absent in that region.[19]

2. Atomic Absorption Spectroscopy (AAS) Studies

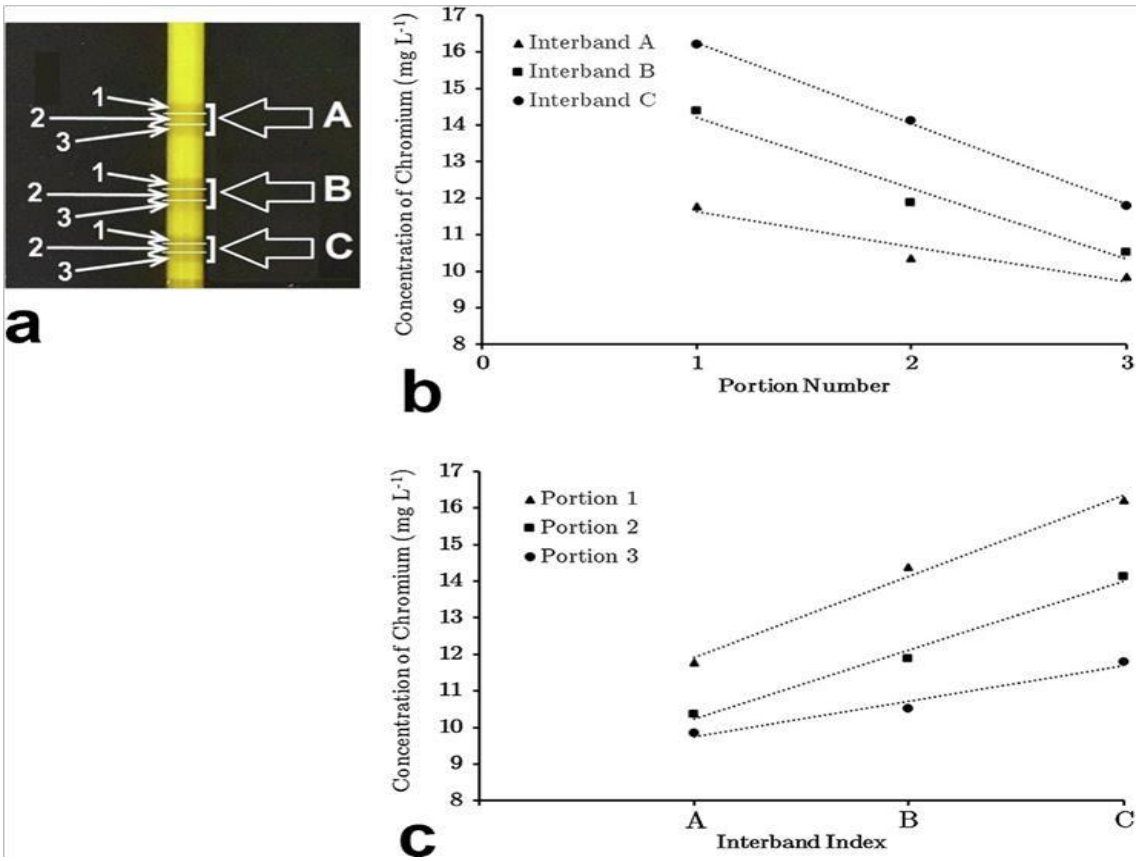

Figure 6. Atomic absorption analysis measurements for the first three consecutive interband gel regions A, B and C. (a) A display of the gel regions selected for measurements. Each interband region is cut into three equal portions (1, 2 and 3), each portion was analyzed alone. (b) The three curves represent the variation of Cr concentration with gel portion within the same interband regions A (▲), B (▪) and C (•) described in frame a. (c) The three curves illustrate the variation of the concentration of Cr with interband order (A, B, and C) for the same gel portion number portions 1 (▲), 2 (▪) and 3 (•). The relative standard deviation is < 1%.[19]

Fig. 6a shows that each interband region is divided into three portions: an upper, a central, and a lower one corresponds to portion 1, portion 2 and portion 3 respectively. Using Atomic Absorption Spectrometry (AAS), the chromium concentration is measured in each interband region taken separately. The plots in Fig.6b. with a negative slope indicate that within each interband taken alone, the concentration of chromium decreases as we move away from the bottom of the band. We can also notice that the concentration

of chromium is highest in the first portion in each interband region close to the previous band. High chromate concentration was detected near the bottom of the band and this is due to CrO_4^{2-} adsorption on the precipitate. The curves in Fig.6c with a positive slope reveal the concentration of chromium for each numbered portion separately (portions 1, 2, or 3 respectively) from each interband region, as we move down the test tube from interband A to B to C. Adsorptivity of CrO_4^{2-} increases as we move down within an interband since the concentration of chromium is the highest for portion 1 (indicated by highest slope) and is the lowest for portion 3 (indicated by the lowest slope). As we go down a test tube, adsorption increases in a lead chromate exhibiting revert spacing. This contrasts with the situation wherein adsorption decreases, in a copper chromate tube exhibiting direct spacing as shown in a previous work[28].

3. Energy Dispersive X- ray (EDX) Studies

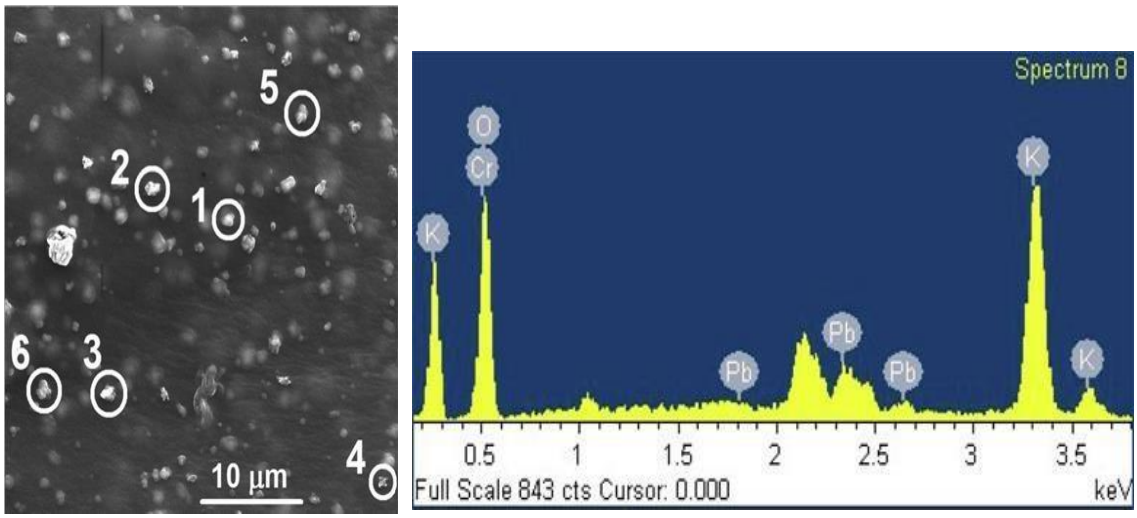

Figure 7. Left frame: Second band bottom with selected particular isolated particles 1 to 6. EDX profile analyzed separately each numbered particle to get the negative/positive charge ratio. The obtained results were recorded in Table 1 Right frame: EDX diffractogram of the particle located in region 5 of the image in the left frame.[19]

Table 1 (shown below) displays the atomic percentages of lead (Pb), Chromium (Cr) and potassium (K) within the particles sticking out in Fig. 7 (left). For Region 5, these are 1.14, 8.94 and 12.84 respectively (see Table 1). As we mentioned earlier, the adsorbed chromate (CrO_4^{2-}) is attracted to the lead ions (Pb^{2+}) to form the lead chromate precipitate, and therefore the Pb^{2+} ions within the particle were neutralized and deposited by chromate ions (CrO_4^{2-}) and their % is 1.14 (Table 1; row 5). Thus the % chromium that remains is 7.80% (1:1 stoichiometry). Now, the remaining chromate ions (7.80%) were neutralized by potassium ions (K^+). The % of potassium required to neutralize all the remaining chromate ions is equal to 7.80 × 2 = 15.6%. As we can notice in the particle, only 12.84% K is present. Therefore, we have 2.76% excess negatively charged chromate left, not being neutralized. Hence, the total negative charge (–) is 15.60

(= 2×Cr left); and total positive charge (K^+) = 12.84 , the ratio is therefore 1.21, which is recorded in the last column of Table 1.[19]

Region	% Pb	%Cr	%K	⊖/⊕(Cr/K)
1	1.55	8.34	14.08	0.96
2	2.11	8.03	12.12	0.98
3	2.42	7.53	10.00	1.02
4	0.91	8.04	13.37	1.07
5	1.14	8.94	12.84	1.21
6	2.52	8.58	10.91	1.11

Table 1. EDX measurements for the six particles selected in Fig. 7. The % remaining Cr (×2)/%K gives the ratio of negative to positive charge, and is recorded in the last column.[19]

This SEM-EDX analysis was performed on 18 randomly isolated particles from the bottom of the second band, but we only report six isolated particles located in different regions as it appeared in Fig. 7 (left). In Table 1, the data recorded represent the atomic % for each of lead, chromium, and potassium in only six randomly selected particles (from 1- 6). From the EDX analysis, we obtain that 12 out 18 (= 66.7%) of the EDX measurements performed the particles have an excess of negative charge. Therefore, during the diffusion process, the overwhelmingly negative charged particles favor the attraction of the positively charged lead ions present in the gel. We also note the presence of potassium ions (K^+) in the organic matrix, but mostly they do not exceed the charge necessary to neutralize the adsorbed chromate ions. Hence, the total charge of the particle will stay negative. Thus, EDX studies confirm the adsorption of chromate ions (CrO_4^{2-}) on the lead chromate precipitate present at the bottom of the

bands.[19] This analysis confirms the role of CrO_4^{2-} adsorption of the precipitate bands in governing the revert spacing in this $PbCrO_4$ Liesegang pattern.

4. Powder XRD

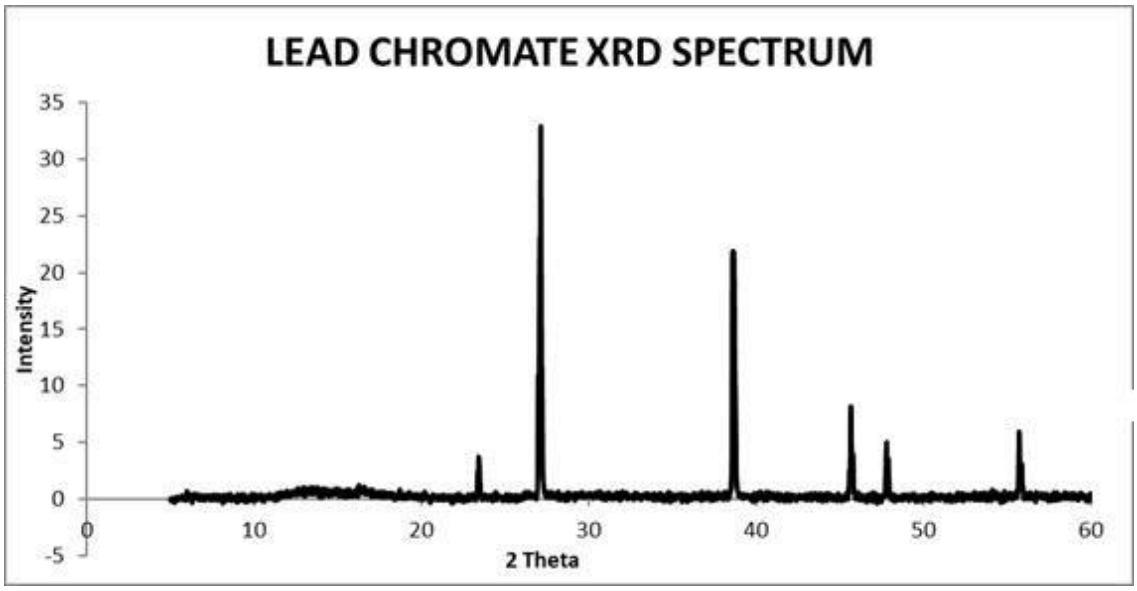

Figure 8. Powder X-ray diffractogram (XRD) of the freeze dried solid lead chromate which is consistent with the monoclinic $PbCrO_4$.

The diffractogram in Figure 8 corresponds to the single monoclinic phase of lead chromate ($PbCrO_4$), confirmed by comparison with the literature[96]. The XRD diffractogram is in perfect agreement with the more stable monoclinic ($PbCrO_4$) polymorph by the significant peak at $2\theta = 27.14°$. The monoclinic form of the lead chromate is more stable than the orthorhombic polymorph.

CHAPTER III

SYNTHESIS AND CHARACTERIZATION OF CALCIUM CARBONATE MINERAL DURING A CARBONATION REACTION, FORGED IN A SLAKED LIME GEL MATRIX

As described in Chapter I, a variety of patterns (rhythmic bands, agates, orbicules…) were observed in geochemistry depending on the mode of reaction-transport processes that occur within a given rock medium. Liesegang banding occurs in a wide variety of natural systems.[2] Several routes can lead to the formation of patterns. Seasonal variations and sedimentation can lead to the formation of physical layering, however not considered as a manifestation geochemical self-organization. Geochemical self-organization can arise from a chemical process that occurs in the wake of a diffusion front.[66-67] Hence, it is the result of the coupling between transport phenomena and chemical reactions.

In this chapter, we present an interesting study on the carbonation reaction of a slaked lime gel matrix mixed homogeneously with calcium hydroxide salt [$Ca(OH)_2$]. This reaction is caused by the diffusion of carbon dioxide coming from two different sources: atmospheric CO_2, and an aqueous solution of carbonic acid (H_2CO_3). Liesegang patterns of calcite [$Ca(CO_3)$] were first observed within a portlandite putty (a simulation of a rock medium) by Rodriguez-Navarro et al.[69]

Guided by this work[69], in our present study we immersed a gel cube matrix of calcium hydroxide [$Ca(OH)_2$]-gel (to which we shall also refer as a putty) into an outer solution of carbonic acid (H_2CO_3). A displacement reaction takes place in the solid phase that converts calcium hydroxide [$Ca(OH)_2$] to calcium carbonate [$Ca(CO_3)$], as follows:

$$Ca(OH)_2\,(s) + CO_2\,(aq) \longrightarrow CaCO_3\,(s) + H_2O\,(l). \qquad \text{(Equation 3.1)}$$

This process engenders the formation of a wide variety of patterns ranging from Liesegang banding to mosaic patterns.[97]

A. Experimental Part

1. Preliminary trials of the carbonation reaction in 2D

In the first stage, we performed experiments to test this carbonation reaction in a 2D petri dish. A sample of $Ca(OH)_2$ (Merck; weighed to the nearest 1.00 g), was dissolved in 100.00 mL of double distilled water with 1% w/w agarose powder (Sigma-Aldrich, Type I, low EEO). The mixture was heated to 90˚C under constant stirring until a homogeneous solution was obtained. The resulting solution was then poured into a set of 2D Petri dishes (2 mm thickness of the putty). The solution was left to cool to room temperature. Then, it is stored for 24 hours. Afterward, on the following day, the putty was sprayed with a phenolphthalein indicator solution (φφ). On the next day, an outer electrolyte of carbonic acid (H_2CO_3) solution having a concentration 0.10 M was gently poured on top of the putty. The system prepared was set aside to age.

2. Putty (lime-agar cuboid) preparation

A sample of $Ca(OH)_2$ (of mass 7.000 g), was dissolved in 700.00 mL of double distilled water with the desired amount of agar powder (Agarose, Sigma-Aldrich A6013, Type I, low EEO), to make 0.135 M $Ca(OH)_2$ in 7.0% w/w gel. The mixture was stirred at 250 rpm for 40 minutes until a homogeneous solution was obtained then heated up to 85°C after adding 30 ml of phenolphthalein. The resulting solution was then left under constant stirring at 250 rpm for around 20 minutes and then poured into a 3D Plexi glass cube of $9\times9\times9 cm^3$, filling it to the rim. The solution was left to gel for 8 hours at 18°**C**.

After gelation, the cube was removed from the mold. Then, the putty obtained was *partially* immersed in 250 ml of the outer electrolyte (H_2CO_3) of concentration 0.10 M. The cube was left uncovered and exposed to air at 18°C.

3. Sample Preparation for powder XRD, FTIR and SEM characterization

a. SEM Imaging

We first used a thin spatula to collect gently samples from the pink (uncarbonated regions) and white (carbonated regions), and then we transferred the gel portions into small vials, ready for freeze drying. Since the pink and white sample portions collected were embedded within the gel matrix, the freeze drying process preserve the texture of the salts needed for analysis. On the next day, the samples were coated with a thin layer of platinum (20 nm thickness) before undergoing SEM.

b. Powder XRD, FTIR, SEM (gel-free)

We first meticulously collected samples from the pink (uncarbonated regions) and white (carbonated regions within bands and white spheres), using a thin spatula, and then transferred each into a 500 ml beaker. Using hot double distilled water (DDW) and centrifugation at 400 rpm for 10 minutes, the obtained gel portions were soaked and washed several times to separate the precipitate from the agar gel matrix and φφ indicator. The supernatant solution was discarded and then the solid samples were left to cool to 18°C. Afterward, in order to obtain a dry powder sample, we left them in a freeze dryer for 24 hours for complete drying. Two fine white powders were therefore obtained, shown in Fig. 9.

Figure 9. White dry powders obtained after the removal of the agarose gel. Left vial (1): solid crystals obtained from the uncarbonated region (pink region); right vial (2): solid crystals obtained from the carbonated regions (white bands and spherulites).

The above two samples were characterized via several techniques: 1. FTIR using the KBr pellet technique, 2. Powder XRD using a diffractometer with a Cu Kα target tube, and 3. SEM using a MIRA3 Tescan electron microscope after coating the samples with a thin layer of platinum (20 nm thickness).

B. Results and Discussion

1. Preliminary 2D Experiments

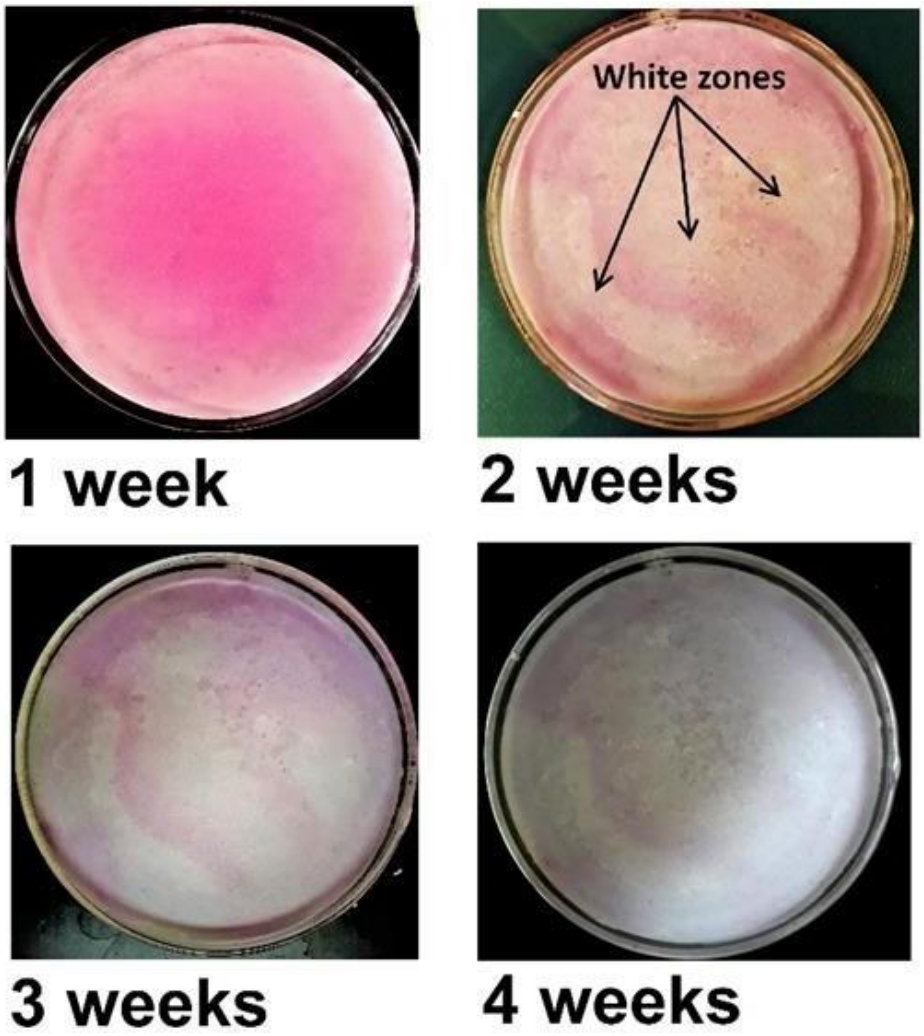

Figure 10. The time evolution of an agarose gel-lime putty undergoing a carbonation chemical reaction. The time is denoted under each figure. Unreacted lime domains (mimicking portlandite $Ca(OH)_2$) are indicated by the pink color of φφ, however, the reacted lime domains (carbonated regions $CaCO_3$) are denoted by the white color.[97]

Figure 10 represents the evolution of an agarose gel-lime putty with time after the putty is subjected to a carbonation chemical reaction (1).

A clear $CaCO_3$ zonation is notably observed on the surface of an agarose gel-lime putty. This is clearly indicated by the white color domains developing between the initially pink putty surface. Some pink regions remain unreacted, indicating the

persistence of calcium hydroxide $Ca(OH)_2$, whereas, other regions undergo the carbonation reaction after sufficient aging, pointing toward the presence of calcium carbonate $CaCO_3$. These latter regions become white in color.

After two weeks, alternating rings of pink and white domains, resembling crescents were clearly observed. According to the Liesegang phenomenon, these rings are similar to real patterning in rocks. This reveals that the carbonation reaction is a slow reaction and is involved in pattern formation. Eleni et al.[80] stated that this carbonation reaction can occur in one of the two following ways: either the calcium hydroxide has completely reacted, or the evaporation of the outer electrolyte. This reaction can be improved by the production of the heat. In 2014, Eleni et al. [80] conducted a comprehensive literature study demonstrating that the % of carbonation in real mortars can reach 80 to 90%.[97] In 2015, Van Balen[98] demonstrated that the % of carbonation reach up to 83%. [97] Based on their studies, two factors play a role in the degree of carbonation the depth within the mortars and its variable chemical composition.[97 98 80]

2. CUBOID

In this section, we are trying to simulate a portlandite rock subjected to a carbonic acid solution (carbonated water) by producing experimentally a gel-$Ca(OH)_2$ cubic putty.[97 99] Initially, the uniform pH of all pink domains is basic (pH =12.1). Fig. 11 represents the diffusion of carbonic acid H_2CO_3 into the gel lime putty and its time evolution.[97]

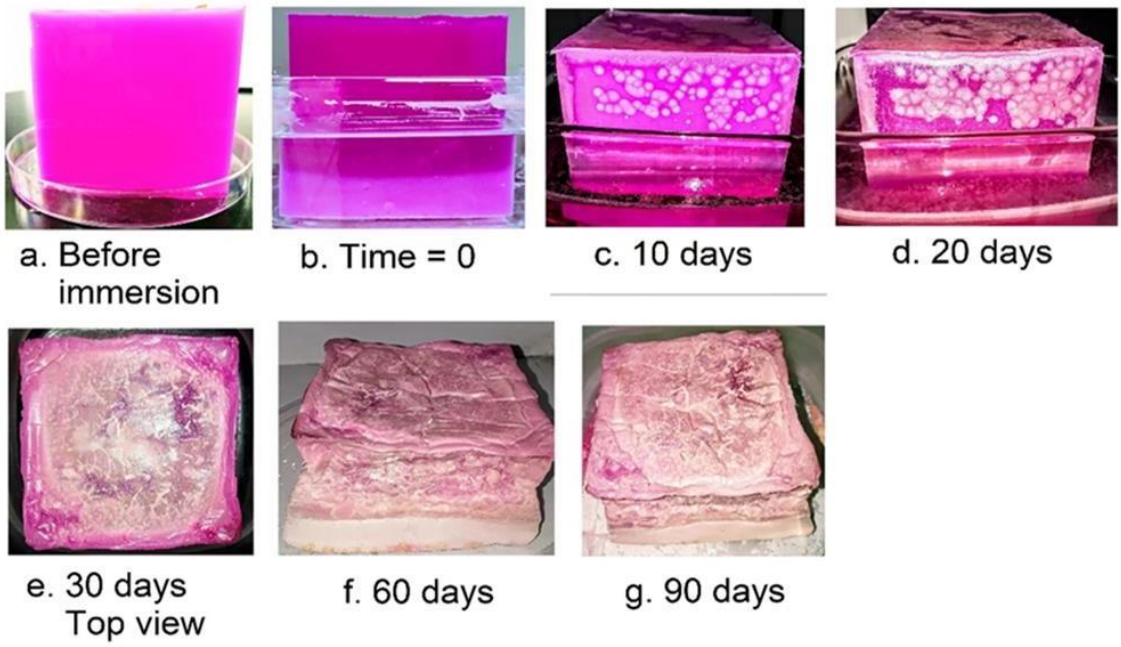

Figure 11. The time evolution of a $Ca(OH)_2$ lime gel putty after the diffusion of carbonic acid solution (H_2CO_3) into it. This is similar to a portlandite rock. The carbonation reaction results in the appearance of white bands and spherulites composed of calcium carbonate. **a-d.** The growth of calcium carbonate precipitates in the form of spherulites and bands after the diffusion of the outer carbonic solution into the putty. **e-g.** Progression and appearance of the rock after the carbonic acid solution has evaporated gradually. Under the photographs, the times are denoted.[97 99]

Behind the diffusion front, we can initially notice a clear white zonation after the carbonation of the putty starts and this is obvious at the bottom of the cube in frames 11b -11d. After a few hours, we can notably observe white spherulites appearing in the upper zones of distinct regions seen in frames 11c and 11d of the putty. These white spherulites are similar to the orbicular texture observed in some rocks. The distribution of the $Ca(OH)_2$ particles which are nonhomogeneous and automatically accumulated more at the bottom of the putty, due to gravity, engenders the formation of spherulites and other mosaic patterns instead of Liesegang bands. Techniques such as further grinding and sonication would not improve the situation much, due to the inevitable time delay necessary for the cooling, and the subsequent gravity effect.

We remark here that the distribution of calcium hydroxide particles in the organic matrix is less erratic at the bottom of the lime gel putty, whereas it becomes more erratic in upper zones, therefore mimicking a porous rock's texture. The horizontality of the H_2CO_3 diffusion front is disrupted by this nonhomogeneous distribution. Frames a-g display the time progression of the lime-gel putty after the complete evaporation of the carbonic acid solution and this will lead to the dehydration of the gel putty. A real rock appearance composed of a mixture of calcite (white zones) and portlandite (pink zones) was also searched for. [97] In similarity between a carbonated lime putty and rhyolitic obsidian rock (real geological system), a coexistence of random spherulites and bands can be clearly discerned [97] (see Figure 12.b)

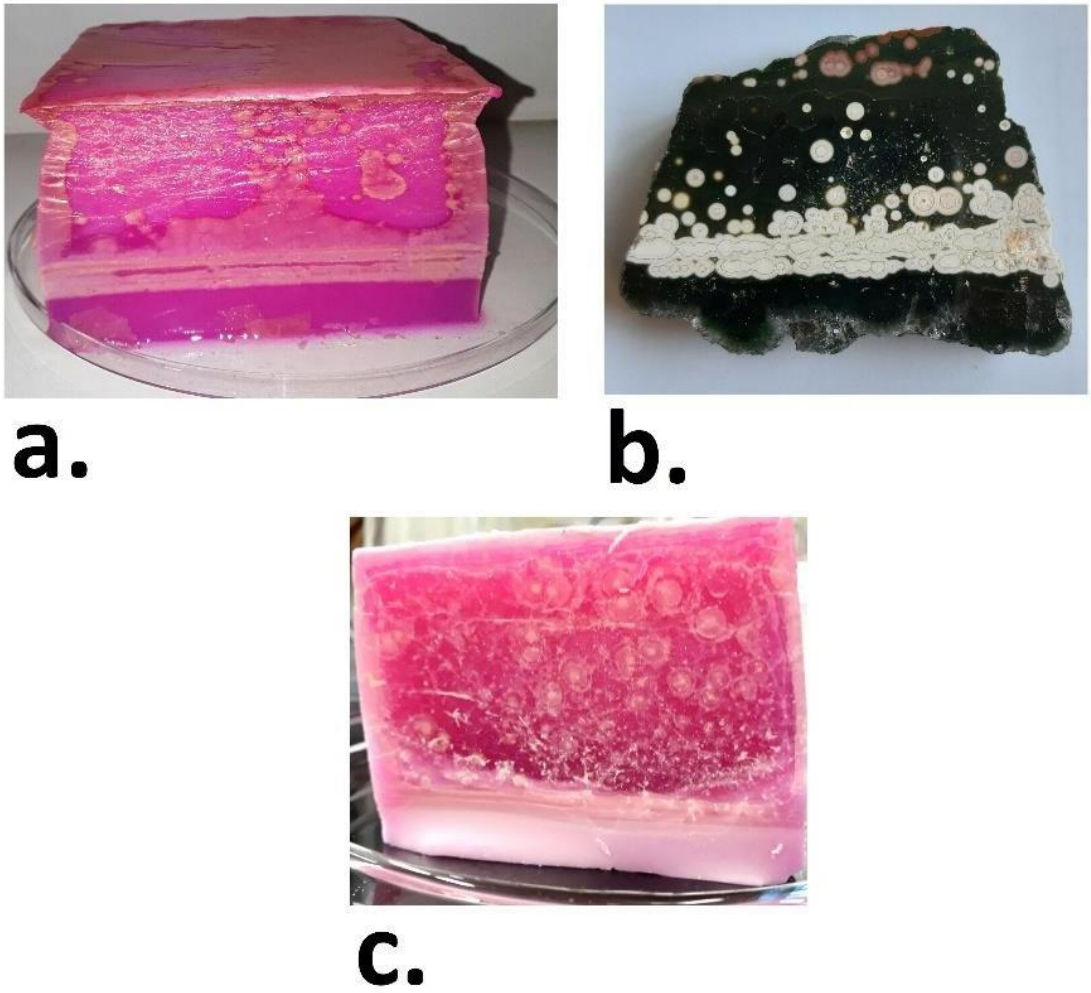

Figure 12. **a.** $Ca(OH)_2$ lime gel putty aged 10 days and exposed to air, presenting bands and spherulites **b.** The coexistence of both random spherulites and bands is similar in both our carbonate putty and rhyolitic obsidian rock **c.** A carbonated putty is presented after a long time, displaying orbicular texture.

.

The two bands at the bottom of our carbonated lime putty (Figure 12. a) are very similar to the white bands present at the bottom of the real rock as shown in Figure 12.b.[97] During an eruption, volcanic gases escaping lead to the formation of spherical vesicles. These latter are filled later with Iron rich calcite (Fe) and calcite ($CaCO_3$, white).[97] Within the putty, white spheroids were displayed very similar to the spherulitic vesicles which appeared with orbicular texture with concentric layers shown in frame 12.c.[97] Congruence in the dynamics of the morphological growth was observed, however the

physicochemical context may be different from our scenario.[97] The extent of carbonation toward close the end is indicated by the heavy white color observed at the bottom of the cube (late times).[80]

C. Characterization of the calcium carbonate zone-patterns

1. pH measurements

At a constant temperature of 18°C, we performed pH measurements of the different regions that appeared on the surfaces of the putty white spheroids, white banded regions and the unreacted pink $Ca(OH)_2$ domains by employing a combination electrode with a flat surface connected to a Thermo-Orion pH meter (model STAR A215).

For each region within the cuboid putty, three pH readings were recorded after 20 days. We obtain the following measurements for the average pH values after 20 days: 11.70 ± 0.03 for the pink domains, 8.35 ± 0.04 for the bottom white bands, and 8.66 ± 0.06 for the white spheres. The values obtained for the carbonated and uncarbonated domains (pH of calcium $Ca(OH)_2$ domain and a $CaCO_3$ domain, 11.7 and 8.5 respectively), are consistent with the values reported in the literature[79-80]. Thus, this verified that a carbonation reaction occurs.

At a specific site on the putty, the time evolution of the pH is in congruence with the percentage of carbonation reaction.[97] Table 2 represents the time evolution of the pH measurements at three distinct regions (white spheres, white bands, and pink zone (uncarbonated regions).[97] A decrease in the pH is a clear trend for the three distinct zones and it is also consistent with the percentage of carbonation.[97]

Location / Time	White spheres	White bands	Pink zone
8 hrs	9.92	Not formed	12.73
10 days	8.93	8.64	12.32
20 days	8.66	8.35	11.70
30 days	8.54	8.13	10.66
60 days	8.36	8.08	10.38
90 days	8.31	8.03	10.31

Table 2. pH measurements at different time intervals at three distinct locations (white spheres, white bands, and unreacted pink regions)[97]

2. SEM Studies

Using SEM, we first investigate the morphology of the freeze-dried crystals present in the white bands over four magnifications: 10 μm, 20 μm, 50 μm, and 100 μm. After samples were freeze-dried, spread on carbon tape, and directly photomicrographed in a scanning electron microscope (MIRA3 Tescan); they are highlighted in frames a-d of Fig. 13 respectively.

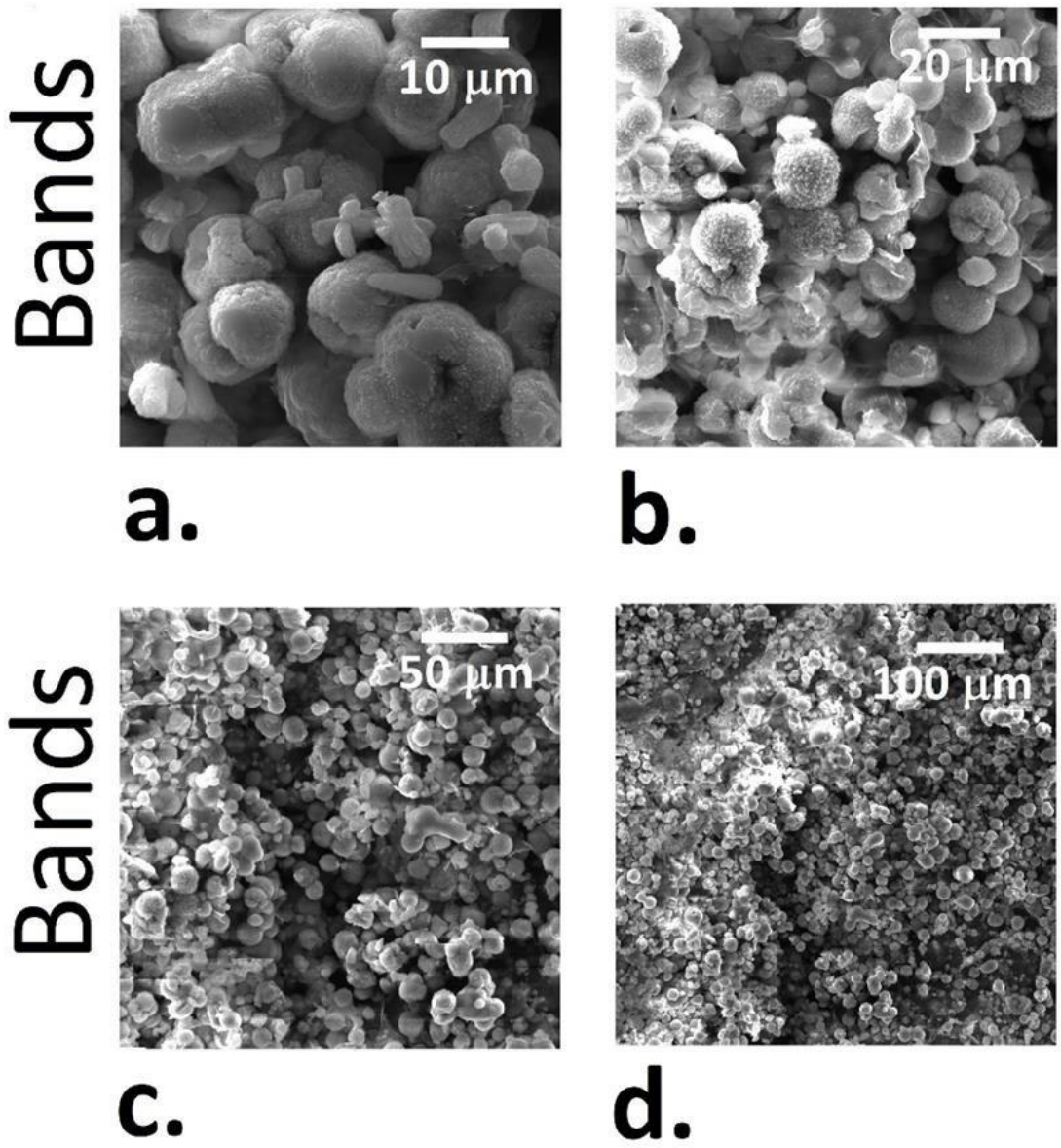

Figure 13. SEM Micrographs of the freeze dried crystals present in the white bands with gel at four different scales appearing on the micrographs. **a.** 10 μm scale; **b.** 20 μm scale; a. 50 μm scale; **d.** 100 μm scale. The rounded shape particles are consistent with amorphous calcium carbonate (ACC). The crystals aggregate on each other in a high density. [97]

Figure 13 shows the texture of calcium carbonate particles $CaCO_3$ embedded within the white bands, typical of Liesegang patterning.[34, 97] These particles correspond to amorphous calcium carbonate (ACC)[100-103] which is characterizing all samples where the agar organic matrix is present since they possess a rounded morphology with a size

ranging between 10 and 20 μm. This is clearly observed in frames 13a and 13b. We can clearly notice the aggregation of $CaCO_3$ particles on top of each other in a high density and this is a well-known characteristic of aggregation within Liesegang bands. [34, 97] These particles are similar to the $CaCO_3$ particles obtained from the crystallization of Na_2CO_3 and $CaCl_2$ in the presence of biopolymer carboxymethyl inulin or CMI, but their size is two to three times bigger (larger calcium carbonate particles).[104] The authors suggested that these particles represent a transition between calcite and calcite + vaterite precipitation. This transition is controlled by two factors: carbonate feeding rate and the biopolymer concentration in solution. [104]

Afterwards, gel samples from the white bands without freeze drying were spread on the carbon tape after a slight exposure to air to conserve a compact layer.[97]

SEM photomicrographs of wet samples extracted from the white bands are displayed in Fig. 14.[97]

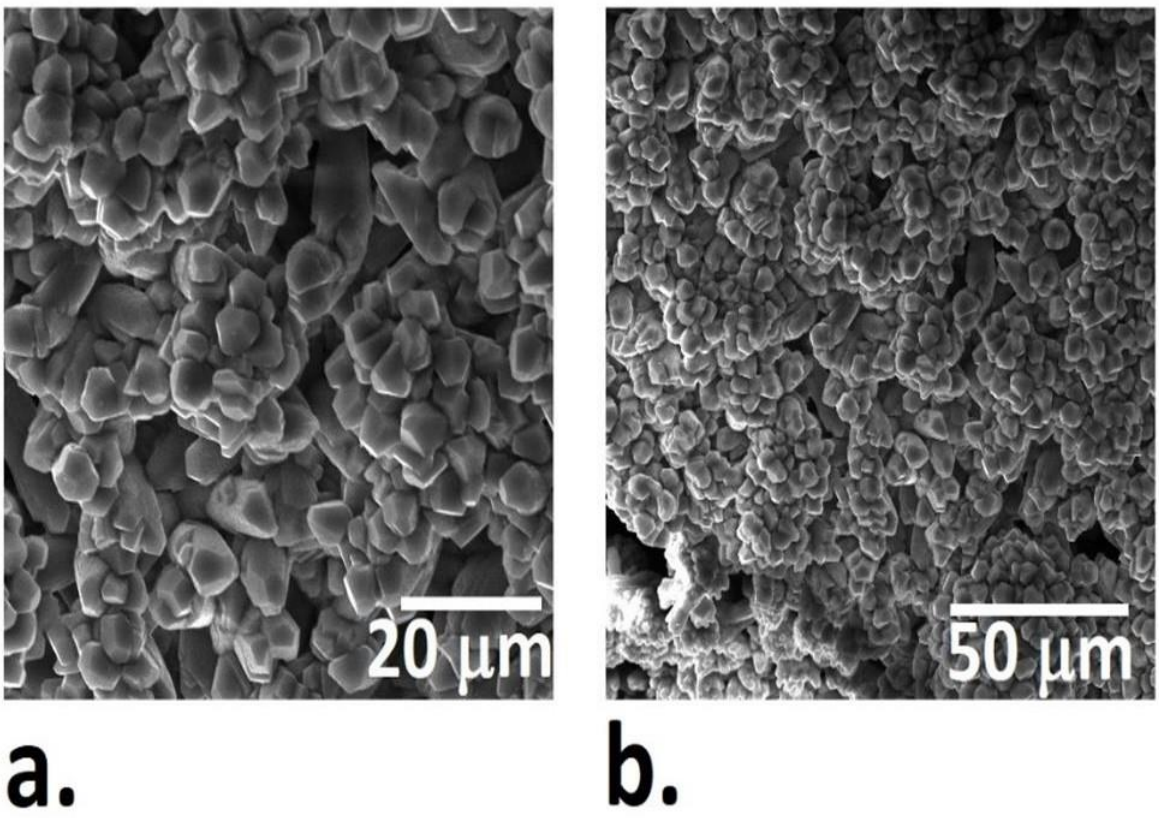

Figure 14. SEM micrographs of the gel aerated particles within the white bands over two different magnifications, show the scale on the micrographs. **a.** 20 μm scale; **b.** 50 μm scale.[97]

As opposed to the SEM images obtained in Fig. 13 where the calcium carbonate crystals were observed as more spherically isolated, we can clearly realize that the particles appear here in a more sticking texture in the presence of the wet gel. Moreover, in terms of morphology, the shape of the crystals in Fig.14 is completely different from that observed in Fig. 13. The particles depart from spherical crystals morphology into a more facetted one[100]. This latter morphology is formed due to the physisorption of water molecules in the presence of a wet organic matrix by the calcium carbonate particles[101]. The morphology in Fig. 14 is that of crystalline calcium carbonate. A dense aggregation of the particles is a typical characteristic of Liesegang banding, but not other typical crystalline arrangements[34]. SEM micrographs of the white calcium carbonate crystals

present in the sphere regions are displayed in Fig. 15 over four different scales: 20 μm scale; 50 μm scale; 100 μm scale; and 200 μm scales[97].

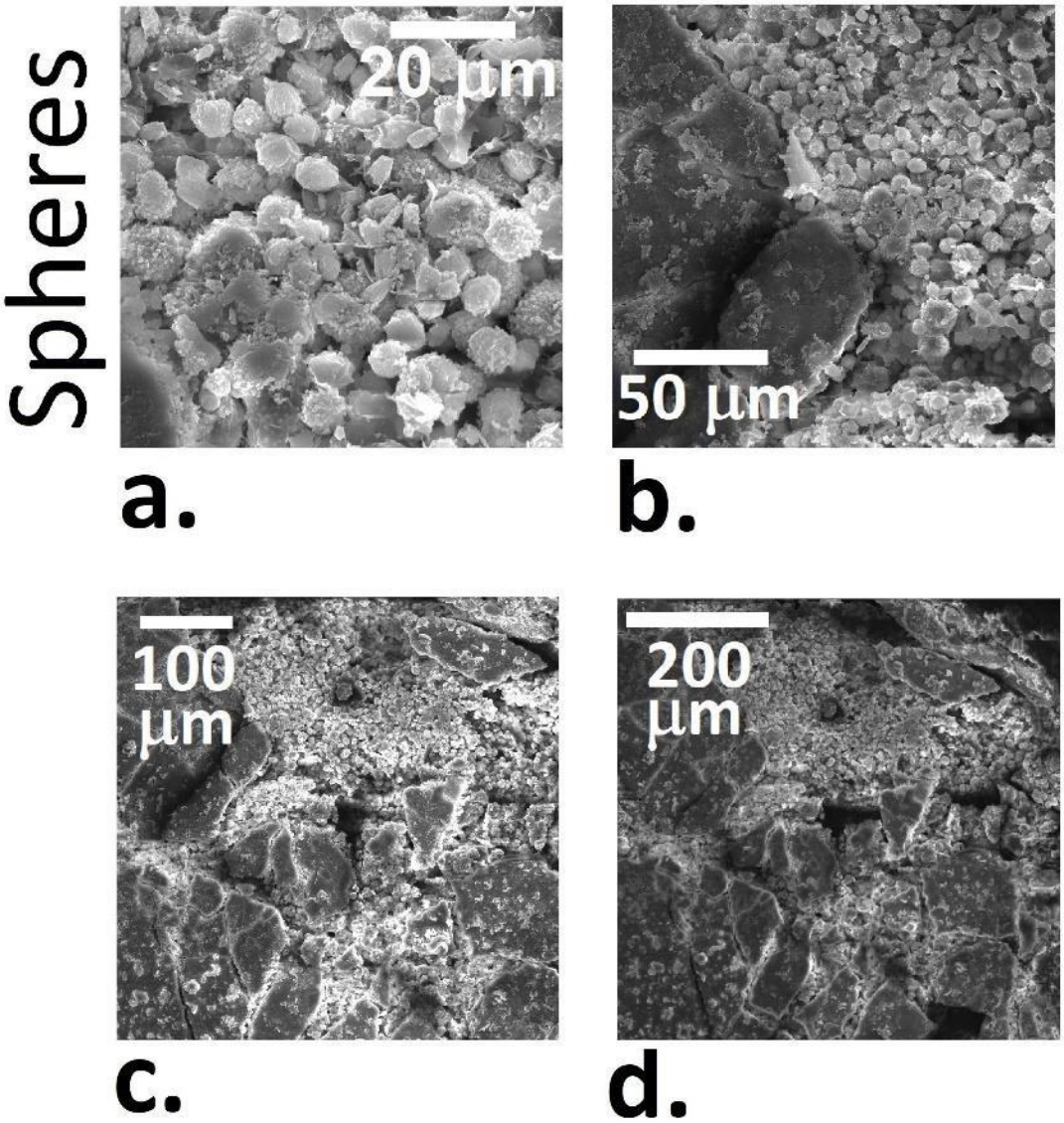

Figure 15. SEM Micrographs of the freeze-dried white crystal within the spheres regions over four different scales **a.** 20 μm scale; **b.** 50 μm scale; **c.** 100 μm scale; **d.** 200 μm scale. The white crystals embedded within the pink bed putty aggregate in islands (frame c and frame d).[97]

We can now clearly observe that the spherical morphology of the calcium carbonate particles is maintained within the spheres regions. This morphology is coined amorphous calcium carbonate (ACC)[103] as previously mentioned. However, within the

spheres, the white crystals aggregate in islands, in contrast with what we previously observed, as a smooth and dense aggregation within the bands (Figs. 13 and Figure 14 respectively). SEM images of the wet gel lime putty are depicted in Fig. 16.[97]

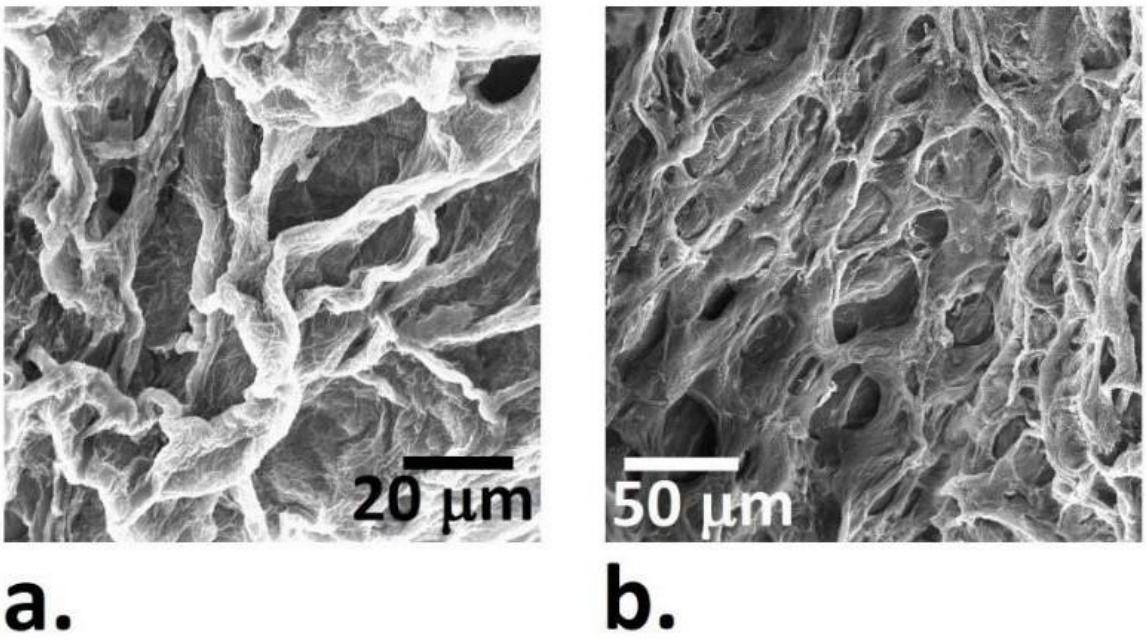

Figure 16. SEM Images of the wet and aerated lime gel putty over two different magnifications **a.** 20 μm scale; **b.** 50 μm scale. The bathing solution (carbonated water) deteriorates the lime gel putty by producing holes and crevices.[97]

The wet aerated pink domains react with the bathing solution (carbonated water) to cause the formation of holes and crevices within the wet pink domains, by deteriorating the wet lime gel putty. In the literature, smooth angles and dissolution patterns were discerned in the SEM figures of carbonated portlandite regions performed in carbonation experiments with supercritical CO_2[105].

Lastly, SEM photomicrographs were performed for the freeze-dried gel-free white solid powder in vial 2 of Fig. 9 after removing the organic matrix from the collected carbonated regions (white spheres and bands) as explained in the experimental section (3.a), followed by freeze-drying.[97]

The texture of these crystals is new and distinct from the ones observed before. We observe a rhombohedral morphology of the calcium carbonate particles appearing in Fig. 17. This morphology is coined *calcite calcium carbonate polymorph*[106]. This latter was also confirmed by powder X-Ray diffraction (XRD), utilizing a Bruker D8 Discover diffractometer with a Cu Kα target tube.[97]

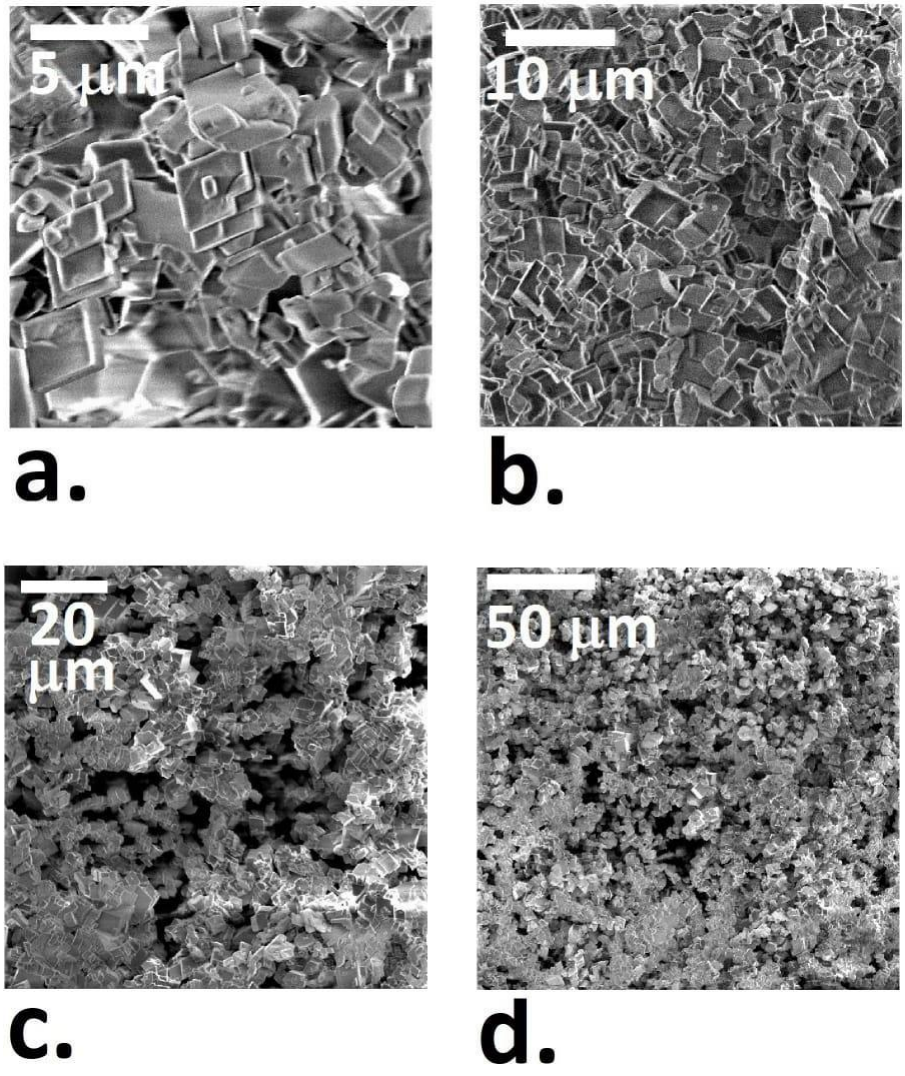

Figure 17. SEM Figures of the white powder (calcite) collected from white bands and spherulites present in vial 2 of Fig. 9 over four different scales **a.** 5 μm scale; **b.** 10 μm scale; **c.** 20 μm scale; **d.** 50 μm scale. This white powder is obtained after the removal of the agarose gel, followed by freeze drying.[97]

3. FTIR Analysis

The two white powders shown in Figure 9 extracted from the pink (basic) and white (acidic) domains, after complete removal of gel were analyzed through FTIR spectroscopy.[97] The crystals collected from the pink (as calcium hydroxide) and white bands and spheres regions (as calcium carbonate) were presented through two spectra.

Frame 18.a. represents the IR diffractogram of the white powder extracted from the pink region ($Ca(OH)_2$) of the gel lime putty (vial 1 in Figure 9). Starting with – OH stretching which is represented by the elongation band at 3690 cm^{-1} and the broad band at 3650 cm^{-1}.[97, 107] Whereas – OH bending is represented by the band at 1440 cm^{-1}.[97] The two vibrations of the Ca-O bond, stretching and bending were shown at 1070 cm^{-1} and 874 cm^{-1} respectively.[107] The IR diffractogram in Figure 18.a. is congruent with the IR diffractogram of calcium hydroxide crystals taken from a reagent-grade bottle.[97]

Frame 18.b. shows the diffractogram of the white powder (vial 2 in Figure 9) obtained from the white domains in the cube (bands and spheres). Calcite mineral is characterized by the presence of carbonate ions (CO_3^{2-}), displayed by the presence of bands at 712 cm^{-1}, 870 cm^{-1}, and 1420 cm^{-1} which represent OCO in-plane bending, asymmetric CO stretching, and out-of-plane deformation respectively.[104]

The broad CO_2 band appearing at 1250 cm^{-1} shadows the latter band (1420 cm^{-1}).[107] Furthermore, high levels of gaseous CO_2 are indicated by the band at 3470 cm^{-1} and the peak at 2510 cm^{-1}.[107] The excessive broadness of the band at around 3500 cm^{-1} is most probably due to absorption by water vapor from the atmosphere. The carbonyl group (C=O bond) from the carbonate appears as a small peak at 1800 cm^{-1} and the two peaks at 2870 and 2980 cm^{-1}.[107] The Ca-O stretching bond is represented by the clearly apparent peak at 1080 cm^{-1}. C-O bond vibration is

attributed to the peak at 712 cm^{-1}. [107] Noted that the IR diffractogram in Figure 18.b, which is characteristic of calcite mineral, matches exactly with that of $CaCO_3$ crystals taken from a reagent grade bottle.[97]

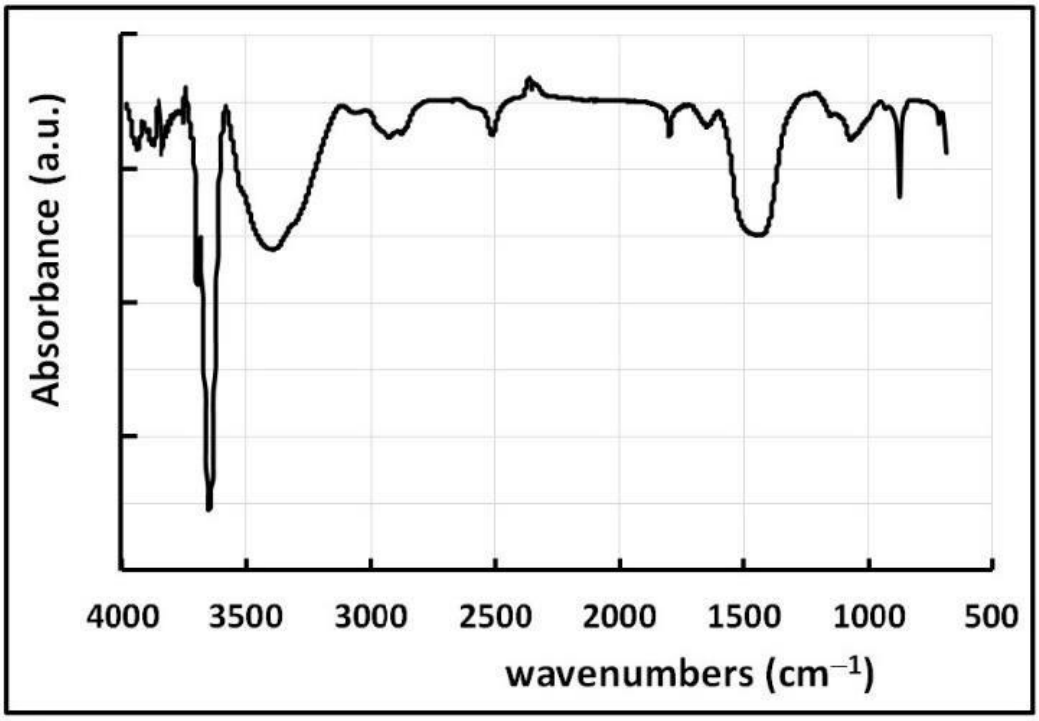

a.

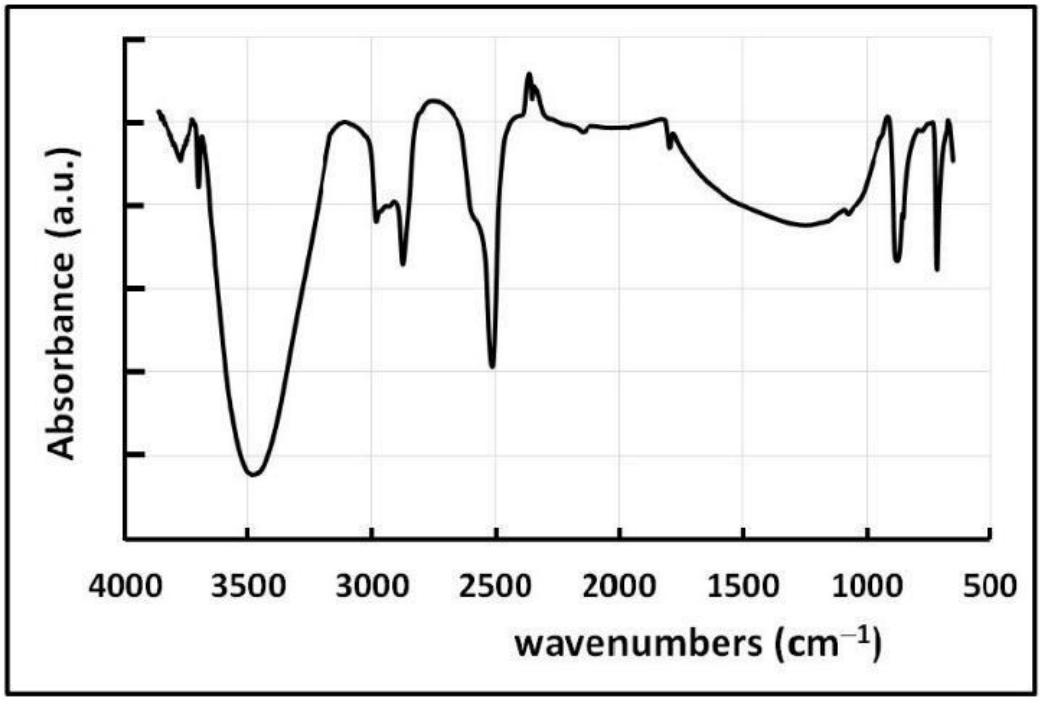

b.

Figure 18 . FTIR diffractogram of freeze-dried white powders a. vial 1 of Fig.9 consistent with $Ca(OH)_2$ (pink domains in the cube) b. vial 2 of Fig.9 is consistent with calcite $CaCO_3$(white domains in the cube)[97]

4. Powder XRD Measurement

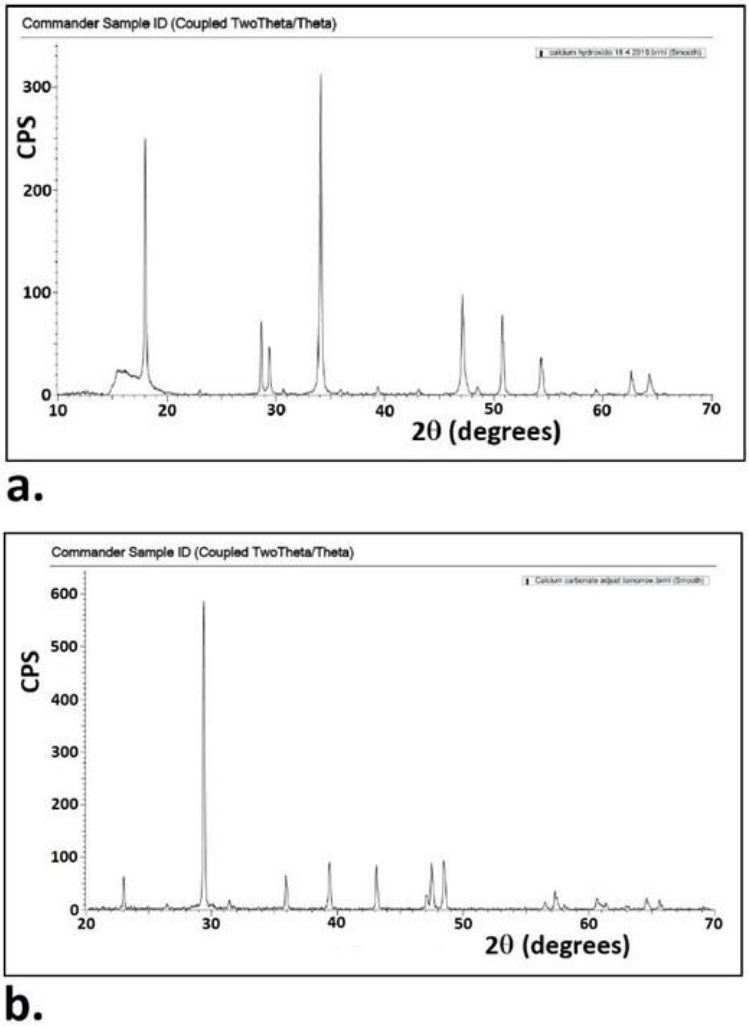

Figure 19. Powder X-ray diffraction (XRD) diffractogram of the freeze-dried solids in vials 1 and 2 of Fig. 9 (pink and white domains) respectively. a. Vial 1: diffractogram consistent with $Ca(OH)_2$; b. Vial 2: diffractogram consistent with calcite mineral $CaCO_3$[97]

The two diffractograms of the white powders present in vials 1 and 2 (Figure 9) are displayed in Figure 19. They were also analyzed by X-Ray diffraction (XRD), using a Bruker D8 Discover diffractometer with a CuKα target tube.[97] The XRD diffractogram in frame 19.a, is in perfect agreement with the diffractogram of calcium hydroxide $Ca(OH)_2$.[97] The diffractogram in frame 19.b represents that of calcite mineral ($Ca\ CO_3$).[97, 104]

From our SEM studies, we realize the departure from amorphous calcium carbonate (ACC) in the presence of the agarose organic matrix to the calcite polymorph (gel-free, freeze-dried calcium carbonate crystals). It is very well-known in the literature that the amorphous calcium carbonate polymorph (ACC) can be transformed into the anhydrous crystalline polymorphs calcite, vaterite, aragonite, or hydrated monohydrocalcite polymorph[108]. Based on many studies found in the literature, the transformation of amorphous calcium carbonate (ACC) into calcite polymorph passes through an intermediate (vaterite or aragonite)[109], and the temperature range at which the conversion between the polymorphs occurs strongly affects the formation of a specific polymorph[109-110]. It is true that the transformation from ACC to calcite experienced here was established by detecting the initial and final polymorphs only (ACC and calcite respectively). We are unable to detect any of the intermediate polymorphs (vaterite or aragonite). [97]

D. Mechanism

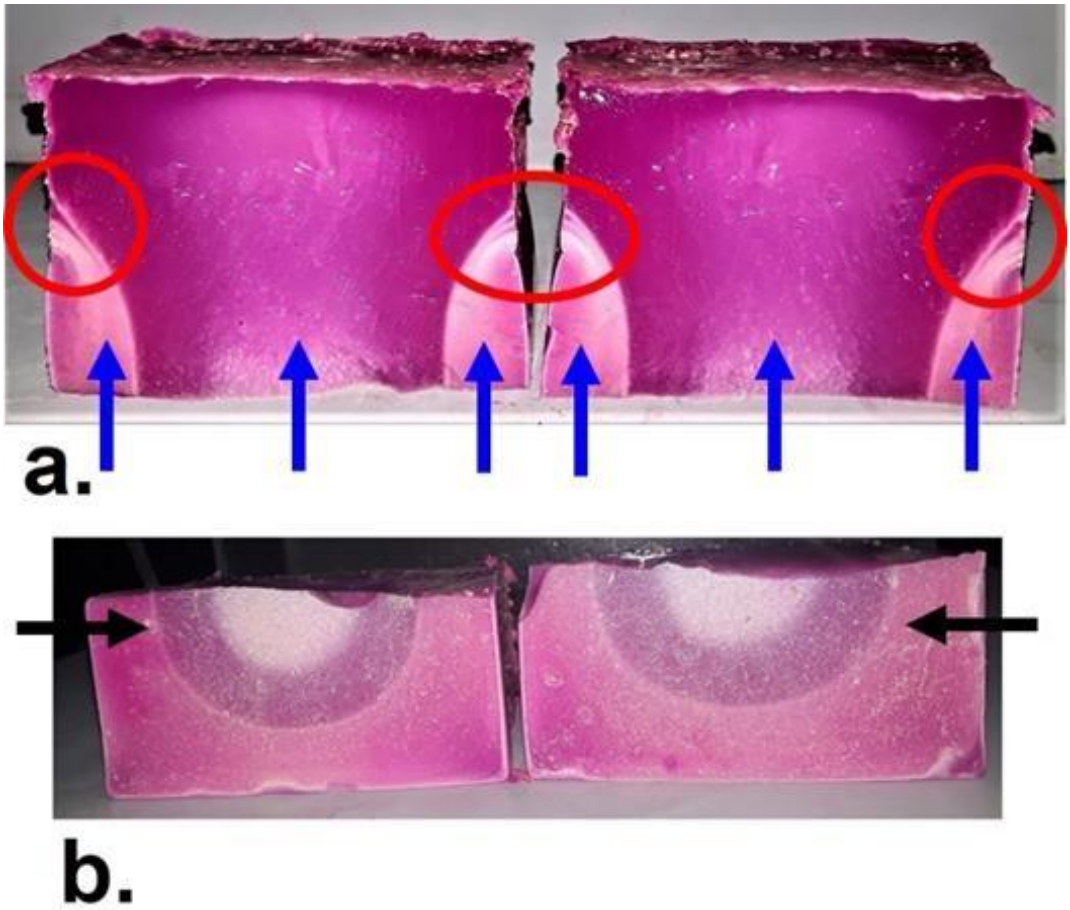

Figure 20. Two cross- sections, longitudinal (a) and transversal (b), of a treated $Ca(OH)_2$ gel cube presenting with a clear zonation. At the center, the upward migrating diffusion front exhibits a mushroom and fingering on the sides. However, the diffusion of the carbonating solution on both sides shows an alteration of $CaCO_3$ and $Ca(OH)_2$ zones. [97]

The formation of the white spherulites only in the upper zones of the cube exposed to atmospheric gases, but bands only at the bottom of the cube in the immersed portion of the putty, will trigger scientists' curiosity to know the mechanism behind their formations. It was clear that there is a notable distinction between bands and spherulites formation. After careful observations, we noticed that the white spherulites were formed only in the upper zones of the cube exposed to the CO_2 present in the air, in the cube portion separate from the immersed part of the putty. Therefore, we can establish that

spherulites' s formation is due to the interaction of calcium hydroxide $Ca(OH)_2$ gel cube with gaseous carbon dioxide (CO_2) according to the reaction:

$$Ca(OH)_2\,(s) + CO_2\,(g) \longrightarrow CaCO_3\,(s) + H_2O\,(l). \qquad (2)$$

This reaction differs from reaction (1) essentially in the phase of CO_2.

Two decisive observations support strongly the above realization: first, when the cube is completely exposed to the air and not immersed at all in the carbonating solution, the white spheres were observed in the upper zone of the lime gel putty. The second observation is when the treated putty, half immersed in a solution of carbonic acid is placed firmly in a closed container, no spheroids are observed.

This clarifies the conclusion that spheroids are formed via the carbonation reaction of the $Ca(OH)_2$ gel cube with the gaseous CO_2 from the air.

In order to understand deeply how the calcium carbonate stratified bands were formed, we performed two cross sections of a treated cube, after a long time, in two directions: one longitudinal and one transversal as shown in Figure 20. Since the $Ca(OH)_2$ gel putty is half immersed, the diffusion of carbonic acid (H_2CO_3) solution from bottom to top (blue arrows) and from both sides (black arrows), resulting in a coupling that leads to the formation of a zonation observed in Figure 20.[97]

As the upward diffusion front of the carbonating solution within the putty reaches the solution surface, bands were observed at the periphery, appearing clearly on the edges of the turning carbonate fingers on both sides (check the red frames).[97] Such intriguing behavior is under continuing study and shows a complex mechanism of the diffusion coupled to carbonation phenomenon.[97]

Lastly, when the cube is fully immersed in an outer electrolyte of carbonic acid (H_2CO_3), the carbonation front penetrates the gel putty homogeneously from all faces.[97] One note

to mention is that a cross-sectional cut of the fully immersed in the carbonating solution displays an essentially uniform light pink (whited region) without any pattern.[97]

CHAPTER IV

CHAOS STUDIES IN 2D $PbCrO_4$ LIESEGANG EXPERIMENTS

Liesegang systems exhibit beautiful precipitate patterns that appear as bands in a 1D test tube or concentric rings in 2D Petri dishes. In a 2D Liesegang experiment, an outer electrolyte from a central source (say NH_4OH) diffuses into a thin layer of gel containing the counter co-precipitate ion (Co^{2+}) leading to the formation of concentric rings $Co(OH)_2$. The most common trend is called the "direct spacing" trend in which the spacing between two consecutive precipitate rings increases as we go away from the circular central junction. The opposite trend is observed in some other systems like lead chromate $Pb(CrO_4)$ (studied here). In a typical Liesegang banding experiment, the total number of patterns increases progressively with time.

As described previously at the end of chapter I, the total number of $Pb(CrO_4)$ patterns (N) in the Pb^{2+}/ CrO_4 system varies erratically under a continuously fed unstirred reactor (CFUR), prompting a chaotic behavior in this variable which is not in conformity with a typical Liesegang banding experiment with a constant diffusion source, without gradual feeding. In a typical 2D $PbCrO_4$ experiment and under a continuous specific flow rate of an outer electrolyte, the variable N undergoes oscillations (band alternations) in an erratic manner. The precipitation reaction is:

$$Pb^{2+}(aq) + CrO_4(aq) \rightleftharpoons PbCrO_4(aq) \qquad \text{(Equation 4.1)}$$

We anticipate that such oscillatory behavior reveals the onset of a chaotic regime, and our observations (reported here) are yet to be characterized as random fluctuations or deterministic chaos.

An interesting example worth mentioning here is that the $Co(OH)_2$ Liesegang periodic precipitation system also presented chaotic behavior. This system exhibits oscillations in the number of bands (N) due to the alternating changes between formation of new bands (precipitation) and disappearance of previously formed bands (redissolution in highly concentrated NH_4OH solution). This latter variable was found to exhibit a chaotic oscillation for all concentrations of cobalt chloride inner solution. These oscillations were demonstrated to be deterministic and chaotic in nature, by standard characterization tools.[93]

In our present study, we will present a preliminary work that studies patterns exhibiting aperiodic or chaotic behavior in the sense that they do not obey the empirical scaling laws.

A. Experimental Section

A sample of $Pb(NO_3)_2$ of concentration 0.0010M (Fluka, 99.0%; weighed to the nearest 0.0165g), was dissolved in 100.00 mL of double distilled water with the desired amount of Bacto agar powder (1% w/w Bacto agar gel). The mixture was heated to 85˚C under constant stirring until a homogeneous solution was obtained. The resulting solution was then poured into a set of 2D Petri dishes of 15 cm diameter, filling each to two-thirds of its height (approximately 80 ml of inner solution). The solution was left to solidify for six hours at room temperature. Initially, an outer electrolyte of concentration 0.20 M (K_2CrO_4; Fluka, 99.0%) was gently poured in the center hole of the lead nitrate doped gel to aliment it initially, and then gradually. The petri dish was then covered and exposed to sunlight at room temperature. Afterwards, a 0.20 M K_2CrO_4 solution was poured initially partially filling the cavity, then at a continuous controlled specific flow rate (see Figure

21). In this experiment, the outer electrolyte is delivered continuously, but at a very slow flow rate. This setup is referred to as a CFUR (continuously fed unstirred reactor).[94]

B. Results

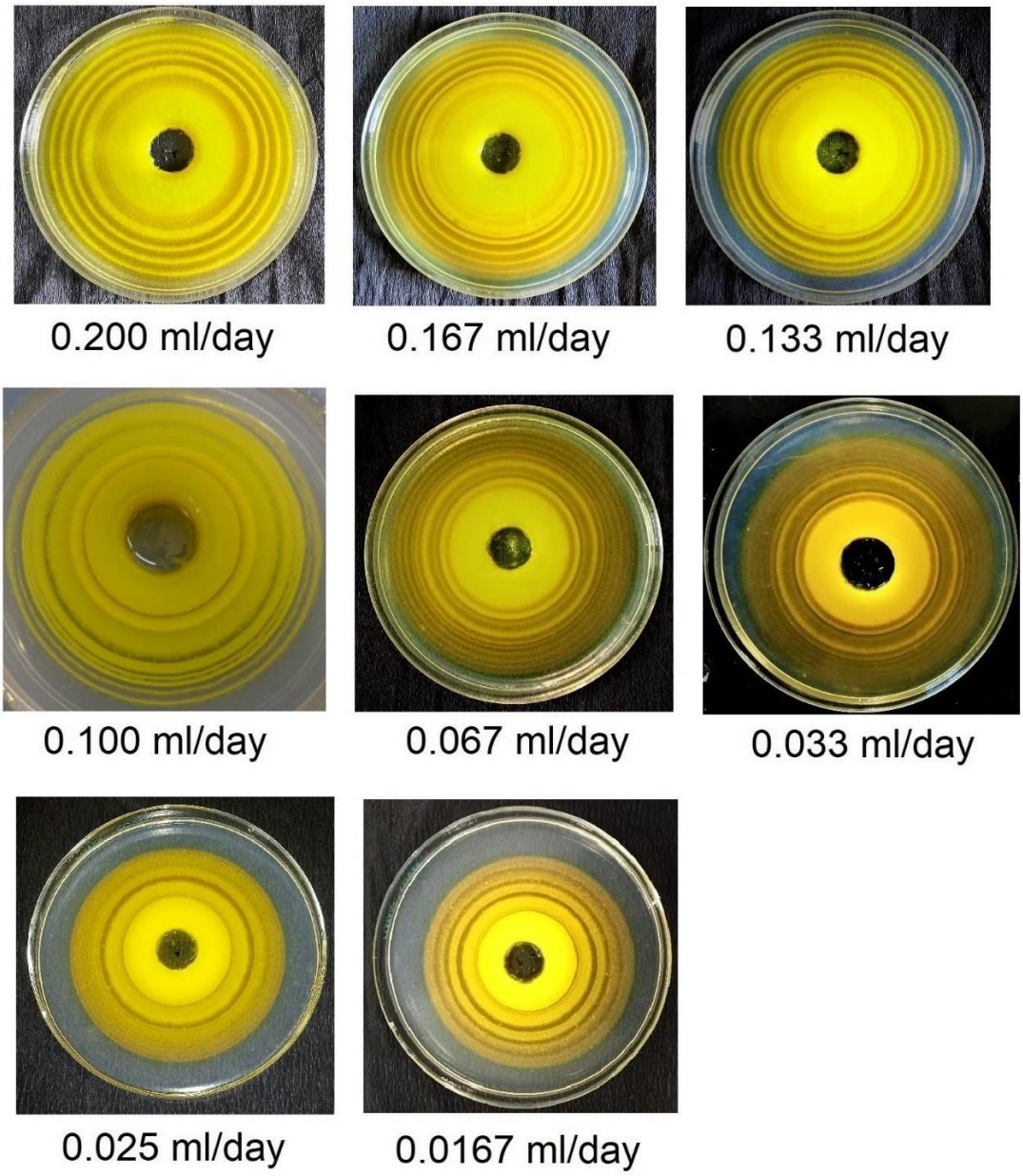

Figure 21. Pattern morphology and variable number of $PbCrO_4$ Liesegang rings (N) for each specific (slow) flow rate with time *t* (days). For all experiments, $[K_2CrO_4]_0 = 0.20$ M. $[Pb^{2+}]_0 = 0.0010$M. Chaotic oscillations of the number of bands *N* at time *t* = 10 days at different flow rates indicated below each frame. For the range (0.100 ml/day - 0.025 ml/day), we observe chaos. Outside this range, periodic behavior is observed.

Flow Rate (ml/day)	Number of bands
0.200 ml/day	6(periodic)
0.167 ml/day	7(periodic)
0.133 ml/day	7 (periodic)
0.100 ml/day	8 (chaotic)
0.067 ml/day	9(chaotic)
0.033 ml/day	9(chaotic)
0.025 ml/day	8(chaotic)
0.0167 ml/day	5 (periodic)

Table 3. Number of rings (N) at time t = 10 days, for different initial flow rates (ml/day).

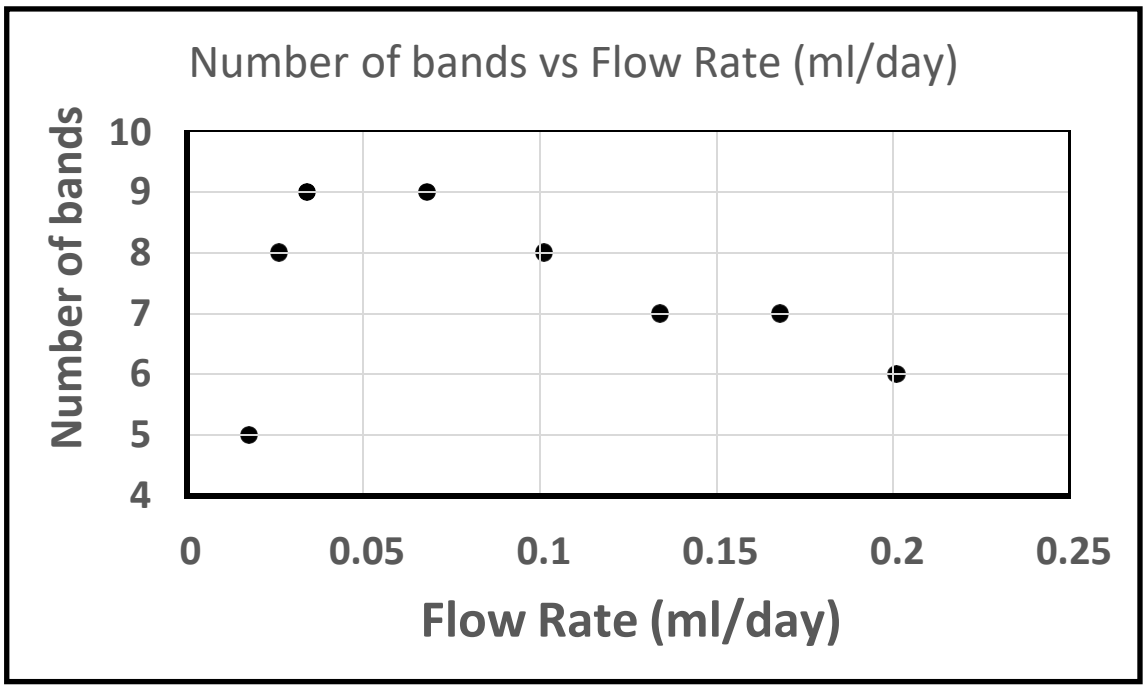

Figure 22. Number of bands (N) vs flow rate (ml/ day) at time t = 10 days for a 2D $PbCrO_4$ pattern.

We carry out a series of experimental runs, using $[K_2CrO_4]_0 = 0.20$ M (outer electrolyte) with $[Pb^{2+}]_0 = 0.0010$M (inner electrolyte). The pattern of bands for each specific flow rate is depicted in Figure 21. We note here that if we start with a relatively low flow rate of outer electrolyte (K_2CrO_4) of 0.100 ml/day, the obtained pattern, in this case, displays a monotonic increase in the number of bands (N) that reaches a maximum of 9 bands for a flow rate of 0.067 ml/days with time, as shown in Table 3 above. Then, this number of bands (N) decreases to reach 5 bands for a flow rate of 0.0167 ml/day. Note that in spite of the apparent periodicity in the variation of the number of bands, the chaotic nature of the pattern lies in the random spatial distribution, the randomness in the spacings, and the chronological order of appearance.

Therefore, to mark the onset of chaos, a control parameter could be the flow rate of the outer electrolyte (potassium dichromate in this case) within a specific observed range. Figure 21 clearly reveals that the randomness in the rings distribution (departure from a

classically periodic Liesegang pattern) starts at a flow rate of 0.100 ml/day spanning a range, reaching a lower edge of 0.025 ml/day. Below the latter flow rate, periodicity is restored. Note here that no standard Chaos characterization could be carried out because of time limitation. The study shall be pursued by successor fellow students.

The plot in Figure 22 shows the variation of the number of the bands (N) with flow rate (ml/day) oscillatory variation. As the flow rate decreases from 0.2 ml/day to half this value (0.100 ml/day), periodic oscillations in the number of bands vs time were initially observed. Every experiment was performed in triplicate and the resulting patterns (compared at the same time) proved to be reproducible. It is such preliminary results wherein exactly the same aperiodic pattern was obtained reproducibly under exactly the same initial conditions, which constitute a preliminary path toward the characterization of the patterns as chaotic. If proved and established by characterization techniques, chaotic behavior starts as flow rate decreases until reaching a threshold value of flow rate of 0.0167 ml/day at which a periodic behavior was recaptured. This plot passes through a maximum at a flow rate of 0.067 ml/day, then returns back to a number of bands of 5 for a flow rate of 0.0167 ml/day, together with the spatial random distribution of the rings. Chaotic behavior is thus observed within the range of outer electrolyte flow rate 0.100 ml/day – 0.025 ml/day. Outside this range, periodic behavior is observed. At high flow rate of outer electrolyte (above 0.2 ml/day), periodic behavior is observed, whereas at flow rates (starting at and lower than 0.100 ml/day), oscillations in the number of bands were observed.

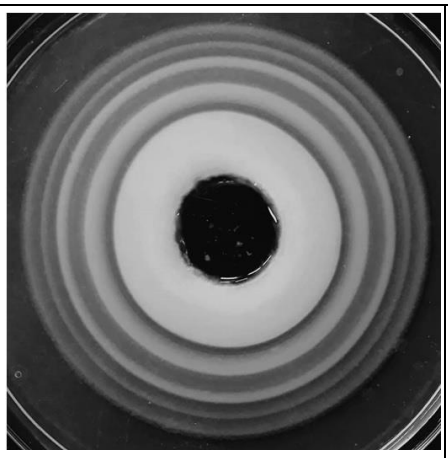

a.

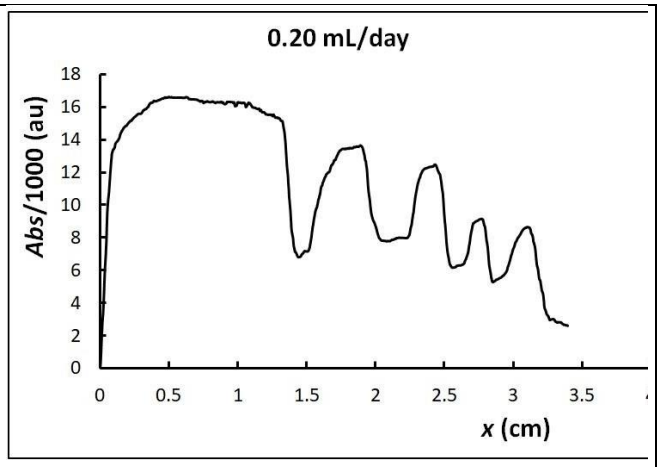
0.20 mL/day
Abs/1000 (au)
x (cm)

b.

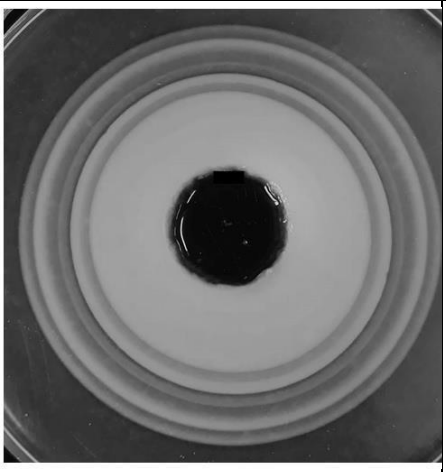

c.

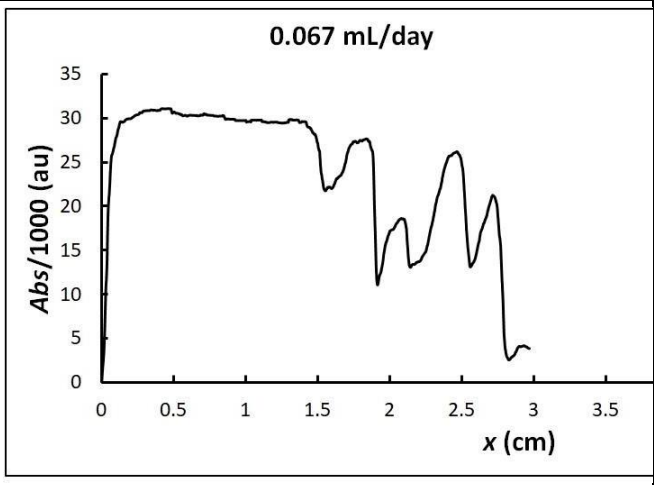
0.067 mL/day
Abs/1000 (au)
x (cm)

d.

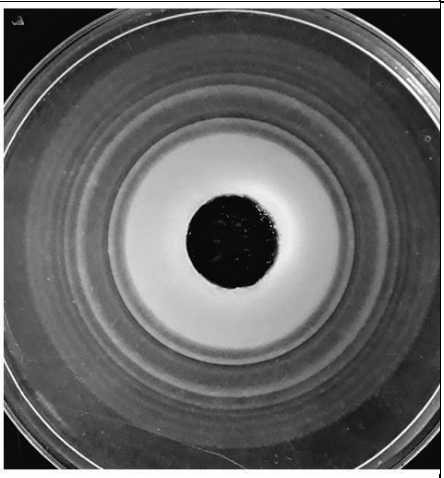

e.

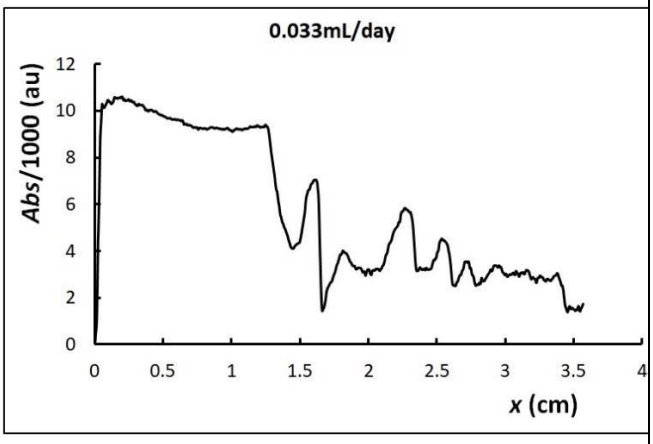
0.033mL/day
Abs/1000 (au)
x (cm)

f.

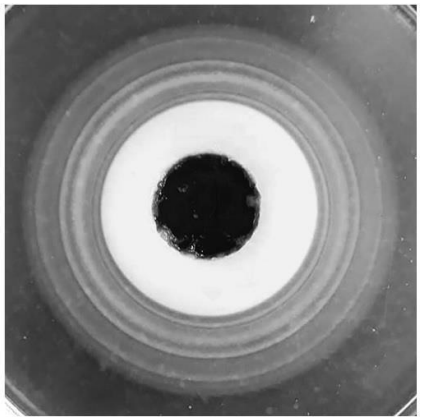

g.

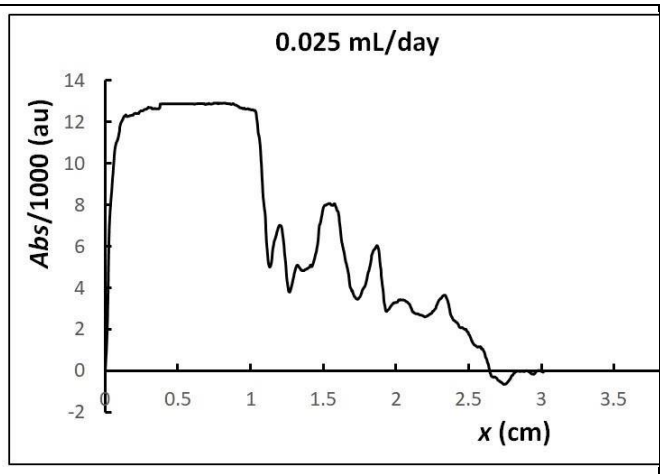

h.

Figure 23. Band maps with the corresponding 2D $PbCrO_4$ Liesegang patterns. **a-b** flow rate = 0.2 ml/day; **c-d** flow rate = 0.067 ml/day; **e-f** flow rate = 0.033 ml/day; **g-h** flow rate = 0.025 ml/day. Chaotic trend increasing with decreasing flow rate above a specific flow rate's threshold value of 0.0167 ml/day. [94]

C. Pattern Characteristics

1. Maps of Rings

At four different flow rates: 0.20, 0.067, 0.033 and 0.025 ml/day, four experiments are highlighted in Fig. 23. Each photograph is digitized using UN-Scanit software, by first mapping the obtained precipitate rings onto a 2D graph of peak intensities.

It is important to note that the net trend for these four flow rates: initially periodic pattern followed by a gradually increasing apparent chaotic trend, then back to periodic pattern again (0.0167 ml/day). These experiments are highly sensitive to flow rate (as initial conditions). A clear comparison between these four experiments can be established by examining the map of rings (frame b, d, f, and h).[94]

2. Number of Bands

As I previously mentioned, chaotic oscillations in the number of bands with time were observed for a specific range of flow rates of outer electrolyte ranging from 0.100 ml/day to 0.0167 ml/day at which periodic behavior was reestablished. Within that range, the number of bands increases monotonically to reach a maximum of 9 bands at a flow rate of 0.067 ml/day in 10 days of experiment. Outside this range, periodic behavior is restored in which 2D $PbCrO_4$ patterns do not present neither a random variation in the spacing between two consecutive bands nor in the width of the rings.

It is important to mention that for all flow rates, one additional band is observed per day, and all the experiments were running in a 15 cm diameter Petri dishes. However, the times for the experiment to end (reach the edge of the dish) differ from one flow rate to another, as shown in Table 5. As the flow rate decreases, the experiment needs more time to terminate and more rings were observed.

Flow Rate (ml/day)	Number of bands (N)	Time (day)
0.20 ml/day	5 bands	5 days
0.067 ml/day	9 bands	9 days
0.025 ml/days	8 bands	8 days
0.0167 ml/days	5 bands	5 days

Table 4. Chaotic Oscillations of the number of bands (N) with time (t) per day for each specific flow rate. As the flow rate decreases, the number of bands increases and more time is needed for the experiment to terminate until reaching a threshold value of 0.0167 ml/day.

3. Band Spacing

Within the same range of flow rate, there is a variation in the spacing between two consecutive bands. The oscillatory variation in the spacings is clearly indicative of transition to chaos due to departure from the trend of a regular Liesegang patterns as shown in Figure 24.

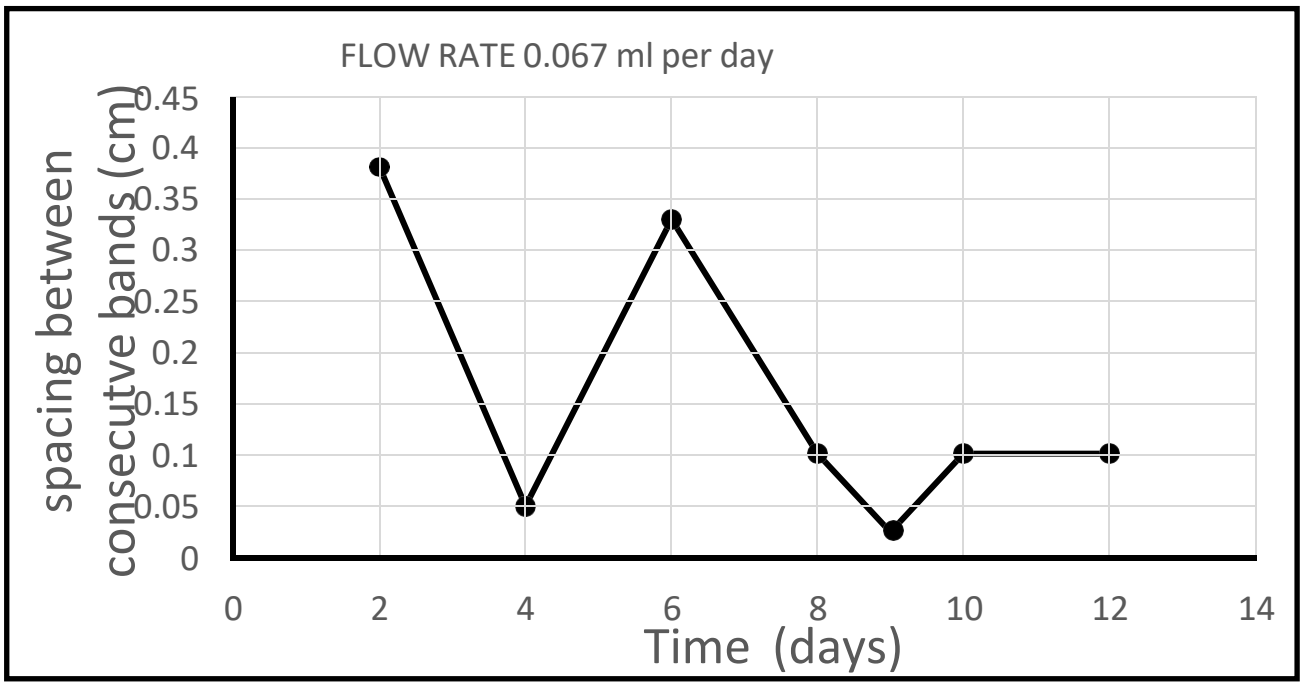

Figure 24. Spacing between consecutive bands vs time (days) for a flow rate 0.067 ml/day in a 2D $PbCrO_4$ pattern.

4. Limitations

This chaotic study presents a number of limitations:

- For a more systematic characterization, power spectrum could not be obtained since one band is forming per day, which is very slow for a chaotic study (a very insufficient time sequence) as compared to cobalt hydroxide system studied by Mustafa Saad et al.[93]
- More runs are required for a chaotic study, but due to the limited size of Petri dishes only few rings (maximum 9 bands were obtained).

- With time, the patterns formed become less clear which makes it harder to identify the rings

CHAPTER V

SUMMARY AND CONCLUSION

The thesis comprised an introduction (Chapter I), in addition to its following three main sections (Chapters II, III, and IV): a novel surface study of revert spacing in a 1D $PbCrO_4$ system (Chapter II); the synthesis and characterization of calcium carbonate mineral via a carbonation reaction, carried out in a slaked lime gel matrix (mimicking a portlandite rock mineral), and leading to pattern formation,; and partially completed chaos studies in 2D Liesegang experiments with $PbCrO_4$ precipitation.

Chapter II was introduced by a full experimental procedure for the preparation of $PbCrO_4$ precipitate patterns. A surface and structural study of a $PbCrO_4$ Liesegang system exhibiting revert spacing was performed. Several techniques SEM, AAS, and EDX were performed to support the role of adsorption of CrO_4^{2-} on the precipitate, in governing the formation of a revert Liesegang pattern. The extent of adsorption of chromate ions on the precipitate was proved to increase as we move away from the outer solution/gel interface. The ascending trend of adsorption favors revert spacing over the direct spacing scenario.

The following outcomes were delineated:

1. EDX studies confirm the adsorption of CrO_4^{2-} on the precipitate.
2. SEM studies display isolated particles, appearing on the finer gel texture of the band bottom. As the band number increases, these isolated particles grow in size, proving an increasing extent of adsorption.

3. AA measurements confirm the absence of CrO_4^{2-} in a given interband region except near the bottom of a band, where more CrO_4^{2-} ions were present in excess, causing the attraction of the Pb^{2+} ions.

An explanation of the mechanism of revert spacing in the $PbCrO_4$ Liesegang system was conducted. In addition, a hypothesis of adsorption of the diffusing outer electrolyte (CrO_4^{2-} ions) on the precipitate bands was tested and confirmed. As the band number increases, the relative adsorption of chromate ions increases. Therefore, this will create a columbic attractive force with the free Pb^{2+}, hence favoring an increase in the rate of adsorption as we move down from the electrolyte junction.

In the second part of the thesis (Chapter III), a study was conducted to investigate the formation of calcium carbonate $CaCO_3$ zonation in a 3D gel cube [$Ca(OH)_2$] putty using a displacement reaction in the solid phase. The obtained calcium carbonate precipitate $CaCO_3$ patterns ranged from Liesegang banding to mosaic patterns. For the characterization of the various differentiated forms within the pattern, and the crystalline forms therein, we used several techniques, namely pH measurements, SEM, FTIR, and XRD. This study pointed out to the fact that the white spherules $CaCO_3$ were formed due to the interaction between calcium hydroxide gel lime putty and the atmospheric gaseous carbon dioxide. Whereas the $CaCO_3$ banding patterns were formed due to the upward diffusion front of the outer electrolyte (carbonated water) within the putty.

In the third and final part (Chapter IV), a preliminary (partial) study was performed to study patterns exhibiting aperiodic or chaotic behavior in the sense that they do not obey the empirical scaling laws. Experiments were performed in 2D Petri dishes on $PbCrO_4$ precipitation, wherein the band distribution trend varies from periodic patterning to deterministic chaos within a flow rate range from 0.025 ml/day - 0.0100 ml/day. Outside this range and on both sides, periodic behavior was observed in the sense that the 2D lead chromate pattern obeys the empirical scaling laws. The study shall be completed by standard characterization methods, but the preliminary results look promising.

REFERENCES

1. Itoh, H.; Wakita, J.-i.; Watanabe, K.; Matsuyama, T.; Matsushita, M., Periodic colony formation of bacteria due to their cell reproduction and movement. *Progress of Theoretical Physics Supplement* **2000,** *139*, 139-151.
2. Sadek, S.; Sultan, R.; Lagzi, I., Liesegang patterns in nature: A diverse scenery across the sciences. *Precipitation patterns in reaction-diffusion systems* **2010,** *661*, 1-43.
3. Moxon, T., *Agate: Microstructure and possible origin*. Terra Publications: 1996.
4. Ortoleva, P. J., *Geochemical self-organization*. Oxford University Press: Clarendon Press: 1994.
5. Stern, K. H., The Liesegang Phenomenon. *Chemical Reviews* **1954,** *54* (1), 79-99.
6. Henisch, H. K., *Crystals in gels and Liesegang rings*. Cambridge University Press: 2005.
7. Liesegang, R., Ueber einige eigenschaften von gallerten. *Naturwissenschaftliche Wochenschrift* **1896,** *10* (30), 353-362.
8. Plath, P. J., Liesegang Structures. In *Imagery Synergetics*, Springer: 2022; pp 45-82.
9. Isemura, T., Studies on Rhythmic Precipitates. *Bulletin of the Chemical Society of Japan* **1939,** *14* (6), 179-237.
10. Sultan, R.; Sadek, S., Patterning trends and chaotic behavior in Co2+/NH4OH Liesegang systems. *The Journal of Physical Chemistry* **1996,** *100* (42), 16912-16920.
11. Shreif, Z.; Al-Ghoul, M.; Sultan, R., Effect of competitive complex formation on patterning and front propagation in periodic precipitation. *ChemPhysChem* **2002,** *3* (7), 592-598.
12. Wagner, C., Mathematical analysis of the formation of periodic precipitations. *Journal of Colloid Science* **1950,** *5* (1), 85-97.
13. Packter, A., The liesegang phenomenon II. Addition of protecting agents. *Journal of Colloid Science* **1956,** *11* (1), 96-106.
14. Chowdhury, D.; Paul, A.; Chattopadhyay, A., Macroscopic and mesoscopic patterns observed in thin films formed due to polymerization of aniline at the air–water interface. *Journal of colloid and interface science* **2003,** *265* (1), 70-76.
15. Morse, H. W.; Pierce, G. W., Diffusion and Supersaturation in Gelatine. *Proceedings of the American Academy of Arts and Sciences* **1903,** *38* (22), 625-648.
16. Nasreddine, V. F. Dissolution fronts and chaotic dynamics in Co (OH) 2 Liesesang systems-by Victor Fuad Nasreddine. 1998.
17. Jablczynski, K., Memoires presentes à la société chimique. Les anneaux de Liesegang. *Bulletin Société Chimie de France* **1923,** *33*, 1592-1602.
18. Antal, T.; Droz, M.; Magnin, J.; Rácz, Z.; Zrinyi, M., Derivation of the Matalon-Packter law for Liesegang patterns. *The Journal of chemical physics* **1998,** *109* (21), 9479-9486.
19. Ezzeddine, D.; El-Rassy, H.; Sultan, R., Surface and structural studies in a PbCrO4 Liesegang pattern with revert spacing. *Chemical Physics Letters* **2019,** *734*, 136735.
20. Mathur, P. B., A Diffusion Mechanism for Liesegang Rings. I. Spacing Law. *Bulletin of the Chemical Society of Japan* **1961,** *34* (3), 437-440.

21. Pillai, K. M.; Vaidyan, V.; Ittyachan, M., On the theory of Liesegang phenomena. *Colloid and Polymer Science* **1980,** *258* (7), 831-838.
22. Ostwald, W.; Hansel, K.; Hammer, G.; Köckritz, U.; Berg, H.; Gröger, M.; Löber, G., Mitteilungen der Wilhelm-Ostwald-Gesellschaft zu Großbothen eV. *Mitteilungen der Wilhelm-Ostwald-Gesellschaft zu Großbothen eV* **2012,** *17* (1).
23. Joglekar, S.; Li, X., Numerical Study of Crystal Growth in Reaction-Diffusion Systems Using Front Tracking. *2019-20 MATRIX Annals* **2021**, 461-471.
24. Smith, D., On Ostwald's supersaturation theory of rhythmic precipitation (Liesegang's rings). *The Journal of chemical physics* **1984,** *81* (7), 3102-3115.
25. Sultan, R.; Ortoleva, P.; DePasquale, F.; Tartaglia, P., Bifurcation of the Ostwald-Liesegang supersaturation-nucleation-depletion cycle. *Earth-Science Reviews* **1990,** *29* (1-4), 163-173.
26. Dee, G., Patterns produced by precipitation at a moving reaction front. *Physical review letters* **1986,** *57* (3), 275.
27. Prager, S., Periodic precipitation. *The Journal of Chemical Physics* **1956,** *25* (2), 279-283.
28. Karam, T.; El-Rassy, H.; Sultan, R., Mechanism of revert spacing in a PbCrO4 Liesegang system. *The Journal of Physical Chemistry A* **2011,** *115* (14), 2994-2998.
29. Kanniah, N.; Gnanam, F.; Ramasamy, P.; Laddha, G., Revert and direct type Liesegang phenomenon of silver iodide. *Journal of Colloid and Interface Science* **1981,** *80* (2), 369-376.
30. Das, I.; Pushkarna, A., Light induced periodic precipitation and chemical instability in lead chromate systems. **1988**.
31. Stern, K. H., *Bibliography of Liesegang rings*. US National Bureau of Standards: 1967; Vol. 13.
32. Mehta, B.; Kant, K., Periodic precipitation of mercury sulphide. *Kolloid-Zeitschrift und Zeitschrift für Polymere* **1966,** *209* (1), 58-60.
33. Kanniah, N.; Gnanam, F.; Ramasamy, P., Revert and direct Liesegang phenomenon of silver iodide: Factors influencing the transition point. *Journal of Colloid and Interface Science* **1983,** *94* (2), 412-420.
34. Lagzi, I.; Ueyama, D., Pattern transition between periodic Liesegang pattern and crystal growth regime in reaction–diffusion systems. *Chemical Physics Letters* **2009,** *468* (4-6), 188-192.
35. Ibrahim, H.; El-Rassy, H.; Sultan, R., Liesegang bands versus random crystallites in Ag2Cr2O7–Single and mixed gelled media. *Chemical Physics Letters* **2018,** *693*, 198-201.
36. Meeks, F. R.; Kosenkranius, H., Determination of the solubility product of CuS in a gel employing the liesegang phenomenon. *Journal of Colloid Science* **1962,** *17* (1), 1-9.
37. Mehta, B.; Kant, K., Formation of Liesegang rings of copper sulphide. *Kolloid-Zeitschrift und Zeitschrift für Polymere* **1966,** *209* (1), 54-56.
38. Kai, S.; Müller, S. C.; Ross, J., Measurements of temporal and spatial sequences of events in periodic precipitation processes. *The Journal of Chemical Physics* **1982,** *76* (3), 1392-1406.
39. Rácz, Z., Formation of Liesegang patterns. *Physica A: Statistical Mechanics and its Applications* **1999,** *274* (1-2), 50-59.
40. Chatterji, A.; Bhagwan, H., Studies on periodic formations: I. Radial rhythmicity. *Journal of Colloid Science* **1958,** *13* (3), 232-236.

41. Bradford, S. C., Adsorptive Stratification in Gels. *Biochemical Journal* **1916,** *10* (2), 169-175.
42. Bolam, T. R.; MacKenzie, M. R., The influence of lyophilic colloids on the precipitation of insoluble salts. Gelatine and silver chromate. Part II. *Transactions of the Faraday Society* **1926,** *22*, 162-177.
43. Sultan, R.; Ortoleva, P., Periodic and aperiodic macroscopic patterning in two precipitate post-nucleation systems. *Physica D: Nonlinear Phenomena* **1993,** *63* (1-2), 202-212.
44. Feeney, R.; Schmidt, S.; Strickholm, P.; Chadam, J.; Ortoleva, P., Periodic precipitation and coarsening waves: Applications of the competitive particle growth modela. *The Journal of Chemical Physics* **1983,** *78* (3), 1293-1311.
45. Feinn, D.; Ortoleva, P.; Scalf, W.; Schmidt, S.; Wolff, M., Spontaneous pattern formation in precipitating systems. *The Journal of Chemical Physics* **1978,** *69* (1), 27-39.
46. Voorhees, P. W., The theory of Ostwald ripening. *Journal of Statistical Physics* **1985,** *38* (1), 231-252.
47. Baird, T.; Braterman, P. S.; Cochrane, H. D.; Spoors, G., Magnesium hydroxide precipitation as studied by gel growth methods. *Journal of crystal growth* **1988,** *91* (4), 610-616.
48. Müller, S. C.; Kai, S.; Ross, J., Periodic precipitation patterns in the presence of concentration gradients. 1. Dependence on ion product and concentration difference. *The Journal of Physical Chemistry* **1982,** *86* (20), 4078-4087.
49. Goldbeter, A., Biochemical Oscillations and Cellular Rhythms (Cam. bridge Univ. Press, Cambridge, UK: 1996.
50. Feeney, R. E.; Petersen, I. M.; Sahinkaya, H., "Liesegang-like" rings of growth and inhibition of bacteria in agar caused by metal ions and chelating agents. *Journal of bacteriology* **1957,** *73* (2), 284-290.
51. Ezzeddine, D.; Sultan, R., Bands, spherulites and 3D zonation in the carbonation of a slaked lime gel matrix. *Journal of Molecular Liquids* **2021**, 117089.
52. Kovács, Á. T., Bacillus subtilis. *Trends in microbiology* **2019,** *27* (8), 724-725.
53. Grammaticos, B.; Badoual, M.; Aubert, M., An (almost) solvable model for bacterial pattern formation. *Physica D: Nonlinear Phenomena* **2007,** *234* (2), 90-97.
54. Shimada, H.; Ikeda, T.; Wakita, J.-i.; Itoh, H.; Kurosu, S.; Hiramatsu, F.; Nakatsuchi, M.; Yamazaki, Y.; Matsuyama, T.; Matsushita, M., Dependence of local cell density on concentric ring colony formation by bacterial species Bacillus subtilis. *Journal of the Physical Society of Japan* **2004,** *73* (4), 1082-1089.
55. Kulkarni, S. D.; Walimbe, P. C.; Ingulkar, R. B.; Lahase, J. D.; Kulkarni, P. S., Revert Banding in One-Dimensional Periodic Precipitation of the (AgNO3+ KBr) System in Agar Gel. *ACS omega* **2019,** *4* (8), 13061-13068.
56. Sibbald, A., Chemical-sensitive field-effect transistors. *IEE Proceedings I (Solid-State and Electron Devices)* **1983,** *130* (5), 233-244.
57. Palaniandavar, N.; Gnanam, F.; Ramasamy, P., Diffusion controlled autocatalytic growth of revert periodic precipitation of cadmium sulphide in lyophillic colloid. *The Journal of chemical physics* **1984,** *80* (7), 3446-3450.
58. Flicker, M.; Ross, J., Mechanism of chemical instability for periodic precipitation phenomena. *The Journal of Chemical Physics* **1974,** *60* (9), 3458-3465.
59. Dietrich, S., Liesegang rings, spirals and helices. In *Spirals and Vortices*, Springer, Cham: 2019; pp 129-140.

60. Abbott, J. E., Studies in periodic crystallization in the absence of a gel. **1933**.
61. Mathur, P. B.; Ghosh, S., Liesegang rings—Part I. *Kolloid-Zeitschrift* **1958,** *159* (2), 143-146.
62. Das, I.; Pushkarna, A., Light induced periodic precipitation and chemical instability in lead chromate systems. *Journal of Non-Equilibrium Thermodynamics* **1988,** *13* (3), 209-220.
63. Das, I.; Pushkarna, A.; Lall, R., Light induced periodic precipitation and crystal growth of PbCro4: A novel study in two-dimensional gel media. *Journal of crystal growth* **1987,** *82* (3), 361-366.
64. Chernavskii, D.; Polezhaev, A.; Müller, S., A model of pattern formation by precipitation. *Physica D: Nonlinear Phenomena* **1991,** *54* (1-2), 160-170.
65. Polezhaev, A.; Müller, S., Complexity of precipitation patterns: Comparison of simulation with experiment. *Chaos: An Interdisciplinary Journal of Nonlinear Science* **1994,** *4* (4), 631-636.
66. Jamtveit, B.; Meakin, P., Growth, dissolution and pattern formation in geosystems. In *Growth, Dissolution and Pattern Formation in Geosystems*, Springer: 1999; pp 1-19.
67. Kruhl, J. H., The Formation of Extensional Veins: An Application of the Cantor—Dust Model. In *Fractals and dynamic systems in geoscience*, Springer: 1994; pp 95-104.
68. Sultan, R. F.; Abdel-Rahman, M., On dynamic self-organization: examples from magmatic and other geochemical systems. *Latin American Journal of Solids and Structures* **2013,** *10* (1), 59-73.
69. Rodriguez-Navarro, C.; Cazalla, O.; Elert, K.; Sebastian, E., Liesegang pattern development in carbonating traditional lime mortars. *Proceedings of the Royal Society of London. Series A: Mathematical, Physical and Engineering Sciences* **2002,** *458* (2025), 2261-2273.
70. Liesegang, R., Chemische fernwirkung. *Photographisches Archiv* **1896,** (801), 331-336.
71. Liesegang, R. E., *Geologische diffusionen*. T. Steinkopff: 1913.
72. Hedges, E. S., Liesegang rings and other periodic structures. **1932**.
73. Götze, J.; Tichomirowa, M.; Fuchs, H.; Pilot, J.; Sharp, Z., Geochemistry of agates: a trace element and stable isotope study. *Chemical Geology* **2001,** *175* (3-4), 523-541.
74. Heaney, P. J.; Davis, A. M., Observation and origin of self-organized textures in agates. *Science* **1995,** *269* (5230), 1562-1565.
75. Boudreaux, A. P., Mineralogy and geochemistry of the Erongo Granite and interior quartz-tourmaline orbicules and NYF-type miarolitic pegmatites, Namibia. **2014**.
76. Owen, J. V., Geochemistry of orbicular diorite from the Grenville Front zone, eastern Labrador. *Mineralogical Magazine* **1992,** *56* (385), 451-458.
77. Berner, R. A., Rate of concretion growth. *Geochimica et Cosmochimica Acta* **1968,** *32* (5), 477-483.
78. Sellés-Martínez, J., Concretion morphology, classification and genesis. *Earth-Science Reviews* **1996,** *41* (3-4), 177-210.
79. Holland, R.; Kurtis, K.; Kahn, L., Effect of different concrete materials on the corrosion of the embedded reinforcing steel. *Corrosion of Steel in Concrete Structures* **2016**, 131-147.

80. Despotou, E.; Shtiza, A.; Schlegel, T.; Verhelst, F., Literature study on the rate and mechanism of carbonation of lime in mortars/Literaturstudie über Mechanismus und Grad der Karbonatisierung von Kalkhydrat im Mörtel. *Mauerwerk* **2016,** *20* (2), 124-137.
81. Rodrigues, J. D., Liesegang rings in differential deterioration patterns of lime mortars. *Journal of Cultural Heritage* **2016,** *21*, 819-822.
82. Al-Ghoul, M.; Sultan, R., Simulation of geochemical banding: Theoretical modeling and fractal structure in acidization-diffusion-precipitation dynamics. *Physical Review E* **2019,** *100* (5), 052214.
83. Msharrafieh, M.; Al-Ghoul, M.; Zaknoun, F.; El-Rassy, H.; El-Joubeily, S.; Sultan, R., Simulation of geochemical banding I: acidization-precipitation experiments in a ferruginous limestone rock. *Chemical Geology* **2016,** *440*, 42-49.
84. Biswas, H. R.; Hasan, M. M.; Bala, S. K., Chaos theory and its applications in our real life. *Barishal University Journal Part* **2018,** *1* (5), 123-140.
85. Lorenz, E., Predictability: does the flap of a butterfly's wing in Brazil set off a tornado in Texas? . **1972**, p. 181). na.
86. Rössler, O. E., Chaotic behavior in simple reaction systems. *Zeitschrift für Naturforschung A* **1976,** *31* (3-4), 259-264.
87. Rossler, O. E.; WEGMANN, K., Chaos in the Zhabotinskii reaction. *Nature* **1978,** *271* (5640), 89-90.
88. Chaos, E., Frigg, R., & Berkovitz, J. , Explaining Chaos. *The British Journal for the Philosophy of Science* **2001,** *52*, .
89. Florian Wodlei, M. R. H. G. A., Periodic Motion in the Chaotic Phase of an Unstirred Ferroin-Catalyzed Belousov Zhabotinsky Reaction. *Frontiers in chemistry* **8 July 2022**.
90. Saurabh, V. V. B. S. S. S. P. R. G. A. R., Ultrasound assisted continuous processing in microreactors with focus on crystallization and chemical synthesis: A critical review. *Chemical Engineering Research and Design* **June 2022,** *Volume 182*, Pages 273-289.
91. Alzaid, S. S.; Chauhan, R.; Kumar, S.; Alkahtani, B. S. T., A High Order Numerical Scheme For Fractal-Fractional Laser System With Chaos Study. *Fractals* **2022**, 2240183.
92. A Garfinkel 1 , J. N. W., W L Ditto, M L Spano, Chaos control of cardiac arrhythmias **1995** 76-80.
93. Mustafa Saad, A. S., and Rabih Sultan*, Revisited Chaos in a Diffusion–Precipitation–Redissolution Liesegang System.
94. Sultan, D. E. R., Mosaic Patterns in Reaction-Diffusion Systems. *Part of the Springer Proceedings in Complexity book series* **8 February 2020**.
95. Kalash, L.; Farah, H.; Eddin, A. Z.; Sultan, R., Dynamical profiles of the reactive components in direct and revert Liesegang patterns. *Chemical Physics Letters* **2013,** *590*, 69-73.
96. Peng, H.; Guo, J.; Li, B.; Liu, Z.; Tao, C., High-efficient recovery of chromium (VI) with lead sulfate. *Journal of the Taiwan Institute of Chemical Engineers* **2018,** *85*, 149-154.
97. Ezzeddine, D.; Sultan, R., Bands, spherulites and 3D zonation in the carbonation of a slaked lime gel matrix. *Journal of Molecular Liquids* **2022,** *346*, 117089.
98. Van Balen, K., Carbonation reaction of lime, kinetics at ambient temperature. *Cement and concrete research* **2005,** *35* (4), 647-657.

99. Ezzeddine, D.; Sultan, R. In *Mosaic patterns in reaction-diffusion systems*, Chaotic Modeling and Simulation International Conference, Springer: 2019; pp 67-74.
100. Gal, A.; Kahil, K.; Vidavsky, N.; DeVol, R. T.; Gilbert, P. U.; Fratzl, P.; Weiner, S.; Addadi, L., Particle accretion mechanism underlies biological crystal growth from an amorphous precursor phase. *Advanced Functional Materials* **2014,** *24* (34), 5420-5426.
101. Konrad, F.; Gallien, F.; Gerard, D. E.; Dietzel, M., Transformation of amorphous calcium carbonate in air. *Crystal growth & design* **2016,** *16* (11), 6310-6317.
102. Reeder, R. J.; Tang, Y.; Schmidt, M. P.; Kubista, L. M.; Cowan, D. F.; Phillips, B. L., Characterization of structure in biogenic amorphous calcium carbonate: Pair distribution function and nuclear magnetic resonance studies of lobster gastrolith. *Crystal growth & design* **2013,** *13* (5), 1905-1914.
103. Xto, J. M.; Borca, C. N.; van Bokhoven, J. A.; Huthwelker, T., Aerosol-based synthesis of pure and stable amorphous calcium carbonate. *Chemical Communications* **2019,** *55* (72), 10725-10728.
104. Kirboga, S.; Öner, M., Investigation of calcium carbonate precipitation in the presence of carboxymethyl inulin. *CrystEngComm* **2013,** *15* (18), 3678-3686.
105. Regnault, O.; Lagneau, V.; Schneider, H., Experimental measurement of portlandite carbonation kinetics with supercritical CO2. *Chemical Geology* **2009,** *265* (1-2), 113-121.
106. Greer, H. F.; Zhou, W.; Guo, L., Reversed crystal growth of calcite in naturally occurring travertine crust. *Crystals* **2017,** *7* (2), 36.
107. Galván-Ruiz, M.; Hernández, J.; Baños, L.; Noriega-Montes, J.; Rodríguez-García, M. E., Characterization of calcium carbonate, calcium oxide, and calcium hydroxide as starting point to the improvement of lime for their use in construction. *Journal of Materials in civil Engineering* **2009,** *21* (11), 694-698.
108. Blue, C. R.; Giuffre, A.; Mergelsberg, S.; Han, N.; De Yoreo, J. J.; Dove, P. M., Chemical and physical controls on the transformation of amorphous calcium carbonate into crystalline CaCO3 polymorphs. *Geochimica et Cosmochimica Acta* **2017,** *196*, 179-196.
109. Rodriguez-Blanco, J. D.; Sand, K. K.; Benning, L. G., ACC and vaterite as intermediates in the solution-based crystallization of CaCO 3. In *New perspectives on mineral nucleation and growth*, Springer: 2017; pp 93-111.
110. Boulos, R. A.; Zhang, F.; Tjandra, E. S.; Martin, A. D.; Spagnoli, D.; Raston, C. L., Spinning up the polymorphs of calcium carbonate. *Scientific reports* **2014,** *4* (1), 1-6.